sure of 1 bar, $Cp^0(T)$ is the heat capacity equation for this mineral for a pressure of 1 bar. The relations between $\Delta_f G^0(T)$ and $\Delta g^0(T)$ are determined by the equality

$$\Delta g^0(T) = \Delta_f G^0(T) + \mathrm{SUM}\{n(i)\Delta g(i)\},$$

where $n(i)$ is the stoichiometric coefficient of element i in its stable state and $\Delta g(i)$ is the free energy of this element at a given temperature [Borisov and Shvarov, 1992].

The heat capacity equation is given as a polynomial in T (it is possible to represent it in the form of a ten-term equation with T in powers of 0, 1, –2, –0.5, 2, 3, 4, –3, 0.5, and –1). If there are phase transitions in a mineral, $Cp^0(T)$ equations are given separately for each temperature interval corresponding to one modification. The last "phase transition" can specify the boundary of the stability field of this mineral.

UNITHERM: calculation of the free energy for reference ions. The calculations of $\Delta g^0(T, P)$ for reference ions (these are usually simple ions with which it is possible to describe the full dissociation reaction of a complex species) were conducted by the modified Helgeson–Kirkham–Flowers (HKF) equation [Helgeson *et al.*, 1981; Shock and Helgeson, 1988; Shok *et al.*, 1989]. Coefficients for most reference ions were borrowed from the SUPCRT92 database [Johnson, Oelkers, and Helgeson, 1992] or later papers by Helgeson *et al.* and other researchers. Now, the coefficients for the direct calculation of $\Delta g^0(T, P)$ with the HKF equation for many solute species are still absent, but there are experimental data involving the determined constant of electrolytic dissociation over certain temperature and pressure intervals. Because of this, in developing the UNITHERM database, we utilized a combined technique for obtaining the thermodynamic data of solute species (it was briefly described by Borisov and Shvarov [1992]), which synthesizes the HKF model and modified Ryzhenko equation [Ryzhenko, 1981; Bryzgalin and Rafal'skiy, 1982; Bryzgalin, 1989].

UNITHERM: calculation of the free energy for complex ions. This part of the UNITHERM database was prepared by Yu.V. Shvarov, M.V. Borisov, and D.V. Grichuk, who developed a technique for the calculation by a semiempirical equation, selected experimental data, assessed their quality, conducted auxiliary calculations, treated the data to attain their consistency, etc.

The $\Delta g^0(T, P)$ for complex ions was calculated by the equation for the dissociation reaction

$$\Delta g^0(T, P) = \mathrm{SUM}\{n(i)\Delta g^0(i)\} - 2.302RT\mathrm{pK}^0_{(\mathrm{diss})},$$

where i are simple (reference) ions, and $n(i)$ are the stoichiometric coefficients of the dissociation reaction. The dependence of $\mathrm{pK}^0_{(\mathrm{diss})}$ on T and P was calculated by the modified Ryzhenko equation

$$\mathrm{pK}^0_{(\mathrm{diss})}(T, P) = (298.15/T)\mathrm{pK}^0_{(\mathrm{diss})}(298, 15\ \mathrm{K}, 1\ \mathrm{bar}) + \mathrm{B}(T, P)(\mathrm{zz/a})_{\mathrm{eff}}, \quad (*)$$

where $\mathrm{B}(T, P)$ is taken to be independent of the character of the ion and can be calculated from $\mathrm{pK}^0(\mathrm{H_2O})$ [under the assumption that $(\mathrm{zz/a})_{\mathrm{eff}}(\mathrm{H_2O}) = 1.0107$] and $(\mathrm{zz/a})_{\mathrm{eff}}$ is a characteristic of the complex ion for which the following approximation is assumed:

$$(\mathrm{zz/a})_{\mathrm{eff}} = \mathrm{A} + \mathrm{B}/T.$$

In comments on each complex ion, characters A through D denote the calculation variant utilized to determine the parameters of this ion. The choice between the variants for the calculation of parameters for Eq. (*) was dictated by the available input information as follows:

(A) If there was a reliable $\mathrm{pK}^0_{(\mathrm{diss})}$ (298.15 K, 1 bar) value for the ion, and there were a few determinations of its pK under other conditions, the value of the $(\mathrm{zz/a})_{\mathrm{eff}}$ was calculated by least-square fitting (LSF) with Eq. (*).

(B) If the $\mathrm{pK}^0_{(\mathrm{diss})}$ (298.15 K, 1 bar) for the ion was unknown or unreliable but its pK was determined under other conditions (for instance, at elevated T), the $\mathrm{pK}^0_{(\mathrm{diss})}$ (298.15 K, 1 bar) and $(\mathrm{zz/a})_{\mathrm{eff}}$ parameters were calculated by LSF with Eq. (*).

(C) If a reliable $\mathrm{pK}^0_{(\mathrm{diss})}$ (298.15 K, 1 bar) value was available but there were no pK determinations under other conditions, the $(\mathrm{zz/a})_{\mathrm{eff}}$ value was calculated as theoretical, following the method of Bryzgalin and Rafal'skiy [1982].

(D) If no $\mathrm{pK}^0_{(\mathrm{diss})}$ (298.15 K, 1 bar) value was available but there was at least one pK determination at other T and P (or a few such values for a narrow interval of P–T parameters), the $(\mathrm{zz/a})_{\mathrm{eff}}$ value was calculated as theoretical, following the method of Bryzgalin and Rafal'skiy [1982], and $\mathrm{pK}^0_{(\mathrm{diss})}$ (298.15 K, 1 bar) was then calculated by Eq. (*).

The reliability of the $\mathrm{pK}^0_{(\mathrm{diss})}$ (298.15 K, 1 bar) values thus obtained diminishes from variant A through D. The wider the P–T interval for which the experimental data on pK were used, the more reliable the extrapolations in variants (A) and (B). Very reliable data were obtained by interpolating experimental data in compliance with the modified Ryzhenko equation.

CHAPTER 2
ESTIMATION OF THE COMPOSITION OF HYDROTHERMAL SOLUTIONS

The assessment of the composition of hydrothermal solutions is one of the most important and limitless problems of research, which is discussed in thousands

of papers and hundreds of monographs with the use of natural data and experimental determinations.

In an effort to develop a genetic model for a certain hydrothermal ore-forming process, the geochemist inevitably faces the problem of selecting a possible composition for the initial solution. The traditional way of resolving this problem involves using data on liquid and gas–liquid inclusions in minerals or experimental data. If there are no data on a certain object, the problem is regarded as having no direct solution and the researcher is left with the possibility of relying on analogies and thermodynamic simulations. However, data on gas–liquid inclusions in minerals from a certain deposit sometimes also fail to provide required information. First, it most often remains unclear as to what was the actual composition of the solutions, because most of the data are of relative character (for example, data on aqueous leachates). Second, practically all of the data characterize one, economically most important interval of the hydrothermal system, namely, the zone of rich ore mineralization, while such genetically important regions of the ore-forming systems as those of the mobilization of ore components and rocks underlying orebodies (which are normally not intersected by mining workings) remain outside the scope of the research. Third, data on inclusions usually do not provide information on the ore potential of these solutions. Fourth, these data cannot give a clue to the origin of components contained in the solutions. Fifth, it remains also uncertain as to what the composition of the initial hydrothermal solution (or solutions) was, because solutions from the ore deposition region could have undergone a long-lasting evolution and significantly modified their composition.

Experimental research is devoid of these disadvantages, because it is conducted under carefully controlled parameters: the composition of the starting and final solutions, temperature, pressure, Eh, etc. However, the main disadvantage of this approach to determining the genesis of hydrothermal deposits stems from the fragmentary character of the data obtained: they cannot describe the whole hydrothermal system, and suitable experiments cannot be found for all natural objects and intervals of conditions.

Thermodynamic simulations can bridge the gaps in the information on inclusions and experimental results obtained on the water–rock system by means of calculations covering regions that cannot be examined directly or are not covered by experimental data. Moreover, the evolution of the solution can be traced, for example, as a function of variations in the external parameters (the technique of multiwave stepwise reactors).

Summarizing this introduction, it is pertinent to mention that estimation of the composition of solutions participating in the origin of hydrothermal deposits can be based on a complex of data, including the results of thermodynamic simulation. This approach was chosen for selecting the solution for the reconstruction of processes responsible for the genesis of vein deposits (Chapters 3–6). This chapter is restricted to the problems of estimating the solution compositions within the framework of thermodynamic simulation (here our approach was pioneering in many respects).

It is necessary to outline the part of the problem of solution composition that was not explored in this research: this is the source of the water itself. Following several researchers, we assumed that water could have come from more than one source (supergene meteoric waters, magmatic, metamorphogenic, and other sources). Here preference is given to the supergene provenance of the bulk of the water with subordinate admixtures of magmatic components (both the water itself and the principal components of hydrothermal solutions: carbon dioxide and chlorine), although they could be provided for the system by rock–water reactions, as was demonstrated by Ryzhenko and Kraynov [2002] and other papers. Other components of hydrothermal solutions could be obtained from rock–water reactions (this will be demonstrated below in this chapter by examples of natural hydrogeochemical systems).

2.1. Method of Boundary Reactions: Estimation of the Composition of Solutions Inducing Various Metasomatic Rock Alterations

The method for quantifying the composition and concentration of the initial solution was described in our earlier papers [Ivanov *et al.*, 1979; Ivanov and Borisov, 1980] using the example of modeling metasomatic zoning in the simplest metasomatic columns controlled by acid leaching. The modeling is underlain by the principles formulated by D.S. Korzhinskii [1969]: (1) the principle of local equilibrium between the rock and pore solution, (2) the principle of the differential mobility of components in metasomatic processes, and (3) the principle of acid–base interaction between the solution and rock.

According to Korzhinskii's theory of metasomatic zoning, infiltration-controlled metasomatism under steady-state conditions results in the progressive growth of metasomatic zones without qualitative changes in their mineralogic composition and rock volume. The zones are separated with sharp replacement fronts and are characterized by a systematic decrease in the number of minerals coexisting in them, up to the transition to a monomineralic rear zone. The inner structure of the metasomatic column is independent of the kinetics of reactions proceeding in it but is determined only by local equilibria at the dissolution and replacement fronts, i.e., at boundaries between the zones.

The technique used to calculate local equilibria at these fronts was as follows. The simulations were conducted for a thoroughly examined natural column of

Table 3. Normative mineral composition (mol %) of the discrete zones of a standard column in quartz–sericite metasomatic rocks

Mineral	Mineral assemblages of zones				
	Qtz	*Qtz + Ser*	*Qtz + Ser + Kfs*	*Qtz + Ser + Kfs + Ab*	*Qtz + Ser + Kfs + Ab + Chl*
Qtz	100	68	65	43	38
Ser	–	32	27	13	8
Kfs	–	–	8	15	20
Ab	–	–	–	30	30
Chl	–	–	–	–	4

metasomatic zones with constant mineral assemblages in the zones and a known succession of the differential mobility of components. Each of the zones was considered to be an open system with perfectly mobile components, for which the set of independent parameters (equilibrium factors) was uniquely specified based on the fact that all of the zones are uniquely related with one another by the regime of the differential mobility of components. By systematically comparing the phase compositions of the neighboring open systems with the lists of perfectly mobile components and the equilibrium factors, boundary reactions at replacement fronts between the zones can be readily deduced [Ivanov and Borisov, 1980]. Following this, the equilibria of these reactions are calculated thermodynamically and examined experimentally, which makes it possible to reproduce the composition of the initial solution and its evolution along the column from zone to zone, with each of which the solution attained local equilibrium.

Consider the simplest, one-act metasomatic column of quartz–sericite metasomatites, which develops during the alteration of granite and whose replacement fronts (zone boundaries) are marked by the incongruent dissolution of aluminosilicate minerals

$$\underset{(5)}{Qtz} \longrightarrow \underset{(4)}{Qtz + Ser} \longrightarrow \underset{(3)}{Qtz + Ser + Kfs}$$

$$\longrightarrow \underset{(2)}{Qtz + Ser + Kfs + Ab}$$

$$\longrightarrow \underset{(1)}{Qtz + Ser + Kfs + Ab + Chl}$$

where (5)–(1) are the numbers of the zones.

Compared with naturally occurring columns, this has no zone with an ore mineral (pyrite, hematite, or magnetite) or calcite, and the zoning did not end with the primary granite.

Under steady-state conditions (constant T, P, and the solution composition and filtration velocity), the following boundary (deduced from the analysis of the mineral assemblages) reactions proceed between the zones:

1–2: $Chl + Kfs + 10H^+ = 3Qtz + Ser + n Mg^{2+} + (5 - n)Fe^{2+} + 8H_2O$;

2–3: $Ab + 0.5Kfs + H^+ = 3Qtz + 0.5Ser + Na^+$;

3–4: $1.5Kfs + H^+ = 3Qtz + 0.5Ser + K^+$;

4–5: $Ser + 10H^+ = 3Qtz + 3Al^{3+} + K^+ + 6H_2O$.

The reactions provide no clue to the salt composition of the solution that determined the differential mobility succession. The solution should be of halide, carbonate, sulfide, sulfate, or other composition or its composition should be complex. This illustrates the convergence of metasomatism, when identical metasomatic zoning patterns can be produced by different initial solutions containing a required set of metals (cations).

The equilibrium solution composition was calculated at 300°C and 0.1–1 kbar for four or, sometimes, five zones, starting from the rear one (monomineralic quartz). The assumed solid phases included all minerals that can be formed at a given bulk composition of the system. The calculations also involved the following aqueous species: H^+, OH^-, K^+, KCl^0, $KHCO_3^0$, KCO_3^-, Na^+, $NaCl^0$, $NaHCO_3^0$, $MgCO_3^0$, HCl^0, Cl^-, CO_3^{2-}, HCO_3^-, $H_2CO_3^0$, Al^{3+}, $Al(OH)^{2+}$, $Al(OH)^{2+}$, $Al(OH)_3^0$, $AlCl_2^+$, $H_3SiO_4^-$, and $H_4SiO_4^0$.

The simulations were based on the principle of the successive saturation of the initial solution in components of the mineral assemblages composing discrete zones of the column with regard for material balance during solution passage through the column. Let us consider a 1-kg portion of each zone and assume that the normative mineralogic composition of the standard reference quartz–sericite metasomatic column is like that presented in Table 3.

We also assume that the rock volumes outlined in discrete zones can interact with 1 kg of water and salts dissolved in it (kinetic aspects of the reactions are ignored). Let the solution in question successively pass through the column. This can be illustrated by the following example. First, we calculate the interaction of

Table 4. Modeling results obtained on zoning in a column of quartz–sericite metasomatic rocks

Initial solution, mol/1000 g H_2O	Metasomatic zones			
	5	4	3	2
H_2O	*Qtz*	*Qtz + Kln*		
H_2O + HCl ($m_{HCl} = 10^{-1}$)	*Qtz*	*Qtz + Kln*		
H_2O + KCl				
$m_{KCl} < 10^{-2}$	*Qtz*	*Qtz + Ser*	*Qtz + Ser + Kfs*	*Qtz + Ser + Kfs + Ab*
$m_{KCl} < 10^{-1}$	*Qtz*	*Qtz + Kfs*	–	–
H_2O + KCl + NaCl ($m_{KCl} + m_{NaCl} = 0.1$)				
(KCl/NaCl) > 1	*Qtz*	*Qtz + Kfs*	–	–
(KCl/NaCl) < 1	*Qtz*	*Qtz + Ser*	*Qtz + Ser + Ab*	–
H_2O + $KHCO_3$ (P_{CO_2} = 1 atm)				
$m_{KHCO_3} = 10^{-5}$	*Qtz*	*Qtz + Kln*	–	–
$m_{KHCO_3} = 10^{-3}$	*Qtz*	*Qtz + Ser*	*Qtz + Ser + Kfs*	*Qtz + Ser + Kfs + Ab*
$m_{KHCO_3} = 10^{-2}$	*Qtz*	*Qtz + Kfs*	–	–

Note: Dashes mean that the zoning pattern has changed during the previous step, because of which the calculations were aborted.

1 kg of pure H_2O with 1 kg of quartz in the rear zone. The entire solution (i.e., water with silica dissolved in it) in equilibrium with the quartz zone is brought to the *Qtz + Ser* zone, in which equilibrium is also attained. The solution that was in equilibrium with the *Qtz + Ser* zone then passes into the *Qtz + Ser + Kfs* zone. Successively transporting the solution from zone to zone, we can trace the changes in the composition of the equilibrium solution at zone boundaries. It should be mentioned that we were the first to utilize the method of stepped flow-through reactors [Ivanov and Borisov, 1980], which was later significantly modernized and tailored for use in the multiwave variant for analyzing complex hydrothermal systems [Grichuk and Borisov, 1983; Grichuk *et al.*, 1985; Barsukov and Borisov, 1987–1992; Grichuk, 2000a].

On completion of reaction interactions with solutions containing certain components in different concentrations, we can determine the boundary variants of the solutions at which the zoning remains unmodified and also check the boundary reactions (at zone boundaries) that were identified above by analyzing mineral assemblages, because we now know the primary (specified) and final (calculated) amounts of these minerals. Thus, we can evaluate the limits in the compositions of the initial solution that result in the development of zoning of a given type.

We examined the following initial solutions: H_2O, H_2O + HCl, H_2O + KCl, H_2O + KCl + NaCl, and H_2O + $KHCO_3$. For each, we calculated local equilibria as described above. The results of simulating zoning in terms of solid phases are summarized in Table 4.

When pure H_2O or H_2O + HCl solution interacted with the *Qtz + Ser* zone, the reaction *Ser* ⟶ *Kln* took place, i.e., a typical argillization (and secondary quartzite) column developed, and a quartz–kaolinite zone appeared between the quartz and quartz–sericite zones.

When a halide H_2O + KCl solution with KCl concentrations from $n \times 10^{-6}$ to $n \times 10^{-1}$ m acts, the following three types of local equilibria can be identified. At m_{KCl} from $n \times 10^{-6}$ to $n \times 10^{-2}$, the standard column is completely reproduced, except for the fact that at $m_{KCl} > n \times 10^{-3}$ albite is dissolved in the *Qtz + Ser + Kfs + Ab* zone according to the reaction *Ab* ⟶ *Kfs*; i.e., albite is leached from the column and replaced by potassium feldspar. An increase in the KCl concentration to 5×10^{-1} m results in the replacement of the *Qtz + Ser* zone, instead of which the *Qtz + Kfs* zone becomes stable, as takes place in natural gumbeites. Because of this, the optimum starting solution for the standard column should have a KCl concentration from $n \times 10^{-6}$ to $n \times 10^{-3}$ m.

If NaCl is introduced into the initial solution containing KCl ($m_{NaCl} + m_{KCl} = 0.1m$), the standard column is also modified. As can be seen from Table 4, the dominance of potassium over sodium gives rise to gumbeite zoning, while opposite relations between these components result in quartz albitite.

In order to estimate the role of a carbonate solution, we calculated three compositions of an H_2O + $KHCO_3$ solution at P_{CO_2} = 1 atm. The standard column remains stable when a solution with $m_{KHCO_3} = 10^{-3}$ acts. At $m_{KHCO_3} = 10^{-5}$, kaolinite appears in the *Qtz + Ser* zone,

Table 5. Variations in the composition of the solution during its passage through a standard column at 300°C

Element, mineral	*Qtz*	*Qtz + Ser*	*Qtz + Ser + Kfs*	*Qtz + Ser + Kfs + Ab*	*Qtz + Ser + Kfs + Ab + Chl*
Si	1.096e–2	1.096e–2	1.101e–2	1.120e–2	1.120e–2
Al	–	2.969e–5	3.077e–6	3.077e–6	3.077e–6
K	1.0e–5	1.992e–5	4.853e–4	1.254e–4	1.254e–4
Na	–	–	–	1.976e–3	1.976e–3
Cl	1.0e–5	1.0e–5	1.0e–5	1.0e–5	1.0e–5
Mg	–	–	–	–	4.0e–8
pH	5.67	6.40	7.99	8.60	8.60

Number of moles of minerals in the zone before (left) and after (right) interaction with the H_2O + KCl solution with $m_{KCl} = 10^{-5}$

Qtz	16.643	16.6321	4.033	4.033*	3.705	3.7063	2.014	2.0187	1.746	1.746*
Ser	–	–	1.866	1.866	1.588	1.5882	0.655	0.6558	0.378	0.378
Kfs	–	–	–	–	0.47	0.4693	0.755	0.7546	0.944	0.944
Ab	–	–	–	–	–	–	1.51	1.508	1.416	1.416
Chl	–	–	–	–	–	–	–	–	0.189	0.189

* Variations are smaller than in the fourth decimal place.

and at $m_{KHCO_3} > 10^{-3}$, potassium feldspar starts to crystallize in the same zone. Because the two latter variants deviate from the standard column, it was senseless to calculate the reactions with farther zones.

It follows that only two of all solutions tested (H_2O + KCl and H_2O + $KHCO_3$) make it possible to completely reproduce the column of quartz–sericite metasomatites, and only within relatively narrow concentration ranges. Since the study with halide solutions were more comprehensive, we consider more closely local equilibria between this solution and the mineral assemblages composing discrete zones of the standard column.

Table 5 illustrates the changes in the initial solution composition (H_2O + KCl) with $m_{KCl} = 10^{-5}$ during its successive passage through the column zones when the velocity of the steady infiltration flow was greater than the rate of component diffusion in the pore solution. The table also reports the variations in the bulk concentrations of elements in this solution as it became saturated with respect to minerals in each zone, pH, and the material balance between the solids and solution.

As can be seen from Table 5 and Fig. 1, the Al and K concentrations in the solution show stepwise changes at the boundaries between zones 5–4 and 4–3 due to the incongruent dissolution of, respectively, sericite and potassium feldspar. The Na concentration exhibits analogous jumps at zone boundary 3–2 due to the incongruent dissolution of albite, and the Mg concentration changes at boundary 2–1 because of the incongruent dissolution of chlorite. All of these changes fully confirm, now on a quantitative basis, the succession of the differential mobility of components. The Si concentration in the solution remains practically unchanged in all zones because of the buffer effect of quartz, which is an excess mineral in all zones. The alkalinity of the solution increases from the rear to frontal zones. The acid–base interaction manifests itself in the stepwise increase in the solution alkalinity (compared with that of the initial solution), while the rock simultaneously becomes more acid (silicic) compared with granite. The Si concentration in the solution is at a maximum and only very insignificantly increases with an increase in the pH of the solution (owing to an increase in quartz solubility). The concentration of Al is three to four orders of magnitude lower than the concentration of Si and decreases with increasing pH. In zones with two (or more) Al-bearing solid phases, the Al concentration in the solution remains unchanged (3.077×10^{-6} m). In zones with two (or more) K-bearing solid phases, the equilibrium solution exhibits a constant $\Sigma K/\Sigma H$ ratio owing to the buffer effect of the univariant *Qtz + Ser + Kfs* association. The Na and Mg concentrations in the solution are stabilized by the buffer effects of albite and chlorite, respectively. It should be stressed that the equilibrium Na concentration in the frontal zones is one order of magnitude higher than the K concentration, although no Na was artificially introduced into the initial solution. Chlorine is a "telescoped" component, whose concentration in the solution does not vary. The loss in the mass of minerals includes their incongruent dissolution and the formation of other stable minerals according to equations for boundary reactions between the zones.

The variants discussed above do not encompass the entire diversity of possible initial solutions that can model the standard zoning.

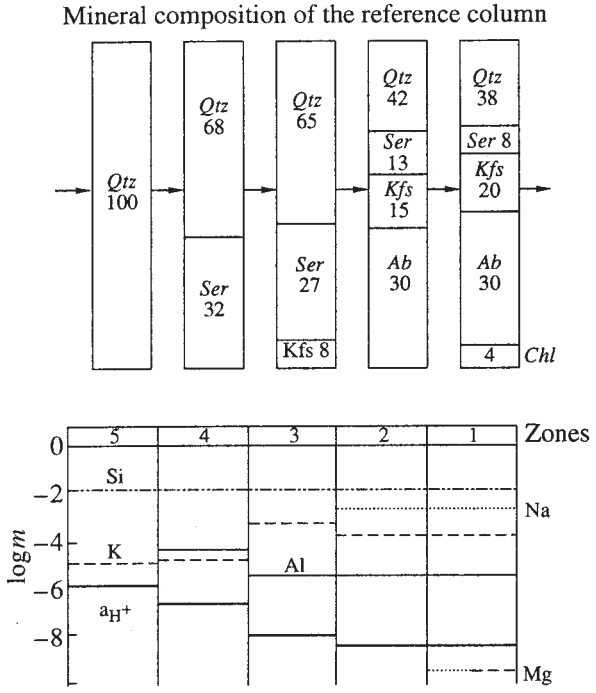

Fig. 1. Bulk concentrations of elements and pH of the solution in equilibrium with mineral assemblages in zones of the quartz–sericite metasomatic column. The initial solution has $m_{KCl} = 10^{-5}$ mol/1000 g H_2O. Mineral assemblages of the zones: (5) *Qtz*, (4) *Qtz* + *Ser*, (3) *Qtz* + *Ser* + *Kfs*, (2) *Qtz* + *Ser* + *Kfs* + *Ab*, (1) *Qtz* + *Ser* + *Kfs* + *Ab* + *Chl*.

2.2. Method of Discrete Reactors: Two Types of Wall-Rock Argillisites

Another approach to estimating the composition of the initial solutions was used in our earlier study of two types of argillisites, which can conveniently be referred to as Si and Al types [Barsukov and Borisov, 1987]. The problem of the development of two distinct types of argillisites (with monomineralic quartz or kaolinite and diaspore rear zones) is of significant geochemical interest.

Problem formulation: zoning in naturally occurring argillisites

A classic argilisite metasomatic column is usually thought to be that of clayey hydrothermal alterations of rocks (most often, granitoids), with a rear zone having a monomineralic quartz composition or approaching it:

(0) granite, (1) *Qtz* + *Fsp* + *Ms*, (2) *Qtz* + *Ms*, (3) *Qtz* + *Kln*, (4) *Qtz*.

Zones between the unaltered granite and quartz–kaolinite rock can also contain other secondary minerals (chlorite, carbonate, and others); the number of these zones can be greater or smaller, but the "common and the most typical feature of all types of acid metasomatism is similar chemical trends of the processes with the removal of all bases from the rocks and the eventual development of rear zones composed only of silica and alumina or even of silica alone" [Zaraiskii *et al.*, 1981].

However, at several deposits rock argillization ends with the development of a rear zone of bimineralic quartz–kaolinite (quartz–dickite) or even more complex composition. There is no exact statistical information on the percentage of currently known argillisites devoid of monomineralic rear zones, and according to indirect data, this type predominates in nature. In any event, most examples described by Yu.V. Kazitsin [1972a, 1972b] and G.T. Volostnykh [1972] are argillisites with bi- and trimineralic assemblages in the rear zones of the metasomatic columns.

Still, monomineralic rear metasomatic zones of wall-rock argillization are known to have developed at several deposits. The most exhaustive information on these deposits pertains to argillisites with rear monomineralic quartz zones, i.e., argillisites with a column of the classical type presented above. Metasomatic aureoles of this type were described by G.T. Volostnykh at rare-metal deposits in the Verkhnyaya Olekma district. Yu.V. Kazitsin documented analogous argilisite columns at the Balei Au–Ag deposit and the Kalangui and other fluorite deposits in Transbaikalia, one chalcedony–pitchblende deposit, rock crystal deposits in the southern Aldan Shield, and some occurrences of ore mineralization in Kamchatka. Analogous argillization columns are also known at "chert" reef U deposits in Butte, Montana; the Morriswail U–fluorite deposit in Utah; and other deposits of the United States.

Much less attention has been paid to the fact that in many instances documented in the literature, quartz is unstable in the inner (adjacent to the selvages) zones of wall-rock argillisites, in which the quartz–kaolinite (quartz–dickite or similar) zones are followed by rear zones composed of kaolinite alone (or dickite, halloysite) or even one of aluminum hydroxide (diaspore, boehmite, or bayerite).

For example, at the Olimpiada fluorite deposit in the Klichka district, eastern Transbaikalia [Shcherban', 1975], F-bearing solutions produced an argillization aureole in granite. The aureole consists of two zones: outer muscovitization and inner kaolinization. At the Chauli U–Mo deposit, Uzbekistan, Barsukov *et al.* [1972] described argillization bands in liparite (and albitized liparite) near pitchblende-bearing veins. The bands consist of two clearly distinct zones: a narrow (1–3 cm) outer grayish green zone of chloritization and carbonatization and a broad (a few centimeters) rear, usually white zone of kaolinization and montmorillonitization. In addition to newly formed chlorite and carbonates typical of the outer zone, it also contains numerous relics of rock-forming minerals and such secondary phases as sericite, iron oxides, sulfides, pitchblende, and coffinite. Much relict material is also preserved in the kaolinite–montmorillonite zone. It was noted that the innermost portions of the "clay" zone

near the selvages contain hardly any quartz (particularly at deep levels of the deposit) and the width of the zone of full quartz dissolution gradually decreases upward from 10–15 cm at paleodepths of 1150–1050 m to 1 cm or less at paleodepths of 900 m and higher [Barsukov *et al.*, 1972].

For another deposit, at which pitchblende and coffinite are associated with fluorite and clay minerals, G.A. Tananaeva [1967] demonstrated that argillization aureoles around mineralized veins in granite porphyry are characterized by a decrease in the SiO_2/Al_2O_3 ratio from 5.04 to 4.74 from the outer to inner zones of the aureoles. However, the mineralized veins and stringers were formed at this deposit in shear fractures, which were originally filled with brecciated wall rocks. Pitchblende, coffinite and other minerals in equilibrium with them metasomatically replaced the finely ground aluminosilicate cement of the breccias, as a result of which the final alteration products of the granite porphyry produced during the mineralizing stage are mineral assemblages in fractures (veins and veinlets) that developed at the expense of ground rock material, for example, halloysite aggregates and bayerite.

An analogous situation was documented at some Hg deposits, at which V.P. Fedorchuk recognized the "dickite (or cinnabar–dickite) type of ore mineralization" and pointed out that "dickite (or kaolinite) is sometimes the only gangue mineral" [Fedorchuk, 1969] that was formed by the metasomatic replacement of the ground cement of breccia zones in schists, sandstones, and acidic volcanics. At the Chempura cinnabar deposit in Kamchatka, the rear zone of the wall-rock argillization in diorite porphyry also has a kaolinite composition. In the Central Kamchatka Ore Province, M.M. Vasilevskii [1973] described a few distinct types of argillization columns in volcanic rocks, including columns of the so-called Ozernovskii type with the following zoning: (0) andesite zone, (1) zone of chloritization and carbonatization, (2)zone of sericitization (or replacement by hydromica), and (3) diaspore zone.

Hence, the analysis of data on the inner structure of natural argillization columns leads to the following two conclusions.

First, rock alterations during medium- and low-temperature wall-rock argillization do not necessarily result in such typical final metasomatic products as monomineralic zones but often end with the development of at least bimineralic (kaolinite + quartz) and, often, even trimineralic assemblages.

Second, if the argillization process does not end with the development of the quartz–kaolinite assemblage, its further evolution can proceed in two distinct ways: either with quartz preservation in the rear zone and the virtually complete dissolution of alumina or, conversely, with alumina retained in the rear zone and the dissolution of quartz or even all silica. *Accordingly, there are two naturally occurring types of wall-rock hydrothermal argillisites, which can be referred to as Si and Al types.*

Different Si and Al behavior in the rear zones of natural argillisites was previously noted by other researchers. Kazitsin [1972a] believed that this is explained by the CO_2 concentration in the solution. On examining fumarolic argillisites, Menyailov and Nikitina [1969] arrived at the conclusion that the differences in the Si and Al behavior are caused not by the concentrations but rather by the composition of the fumarolic gases and their condensates: the Si type of clayey aureoles is formed by sulfuric fumaroles and solutions, whereas the Al type develops under the effect of halide gas jets and their condensates on the rocks.

Based on kaolinite solubility at 25°C, Pokrovskii and Ivanov [1982] and Ivanov [1984] have demonstrated a more realistic and rigorous approach to the problem of Al and Si behavior in argillisites. The development of quartz or diaspore at the expense of kaolinite can be a consequence of the incongruent dissolution of the latter and can depend on the pH of the solution acting on the kaolinite.

We considered the behavior of Si and Al during the development of wall-rock argillisites after granitic rocks at 150°C, which is one of the most realistic estimates for such processes. For this purpose, we created two thermodynamic models for argillisite columns of Si and Al types and determined the limits for the variations in the bulk concentrations of the main components of chloride–carbon dioxide hydrothermal solutions that produced columns of the two types.

Simulation methods and results

Models for argillization columns forming under the effect of solutions of different compositions were devised by calculating local equilibria in the system H–O–K–Na–Ca–Mg–Fe–Al–Si–C–Cl–(S), which is described by 31 solid phases and 50 solute species. All calculations were carried out for isothermal conditions (150°C) and the saturated water vapor pressure.

Inasmuch as medium- and low-temperature hydrothermal solutions are dominated by solutions of chloride–carbon dioxide composition, in the simulations we limited ourselves to discussing only these solutions. The primary rock was taken to be liparite (tuff of quartz porphyry; its analysis is given in Chapter 3) from the U–Mo Chauli deposit.

A decrease in the degree of hydrothermal alteration of the rock from the rear to frontal argillization zones was imitated by a series of calculations with the systematically increasing mass ratio of liparite to water of the acting solution ($m_{rock}/m_{H_2O\ solution}$) or by systematic variations in the reaction progress.

In all of our models for argillization columns, the zero zone was unaltered liparite. Regardless of the variations in the composition of the argillizing acid chlo-

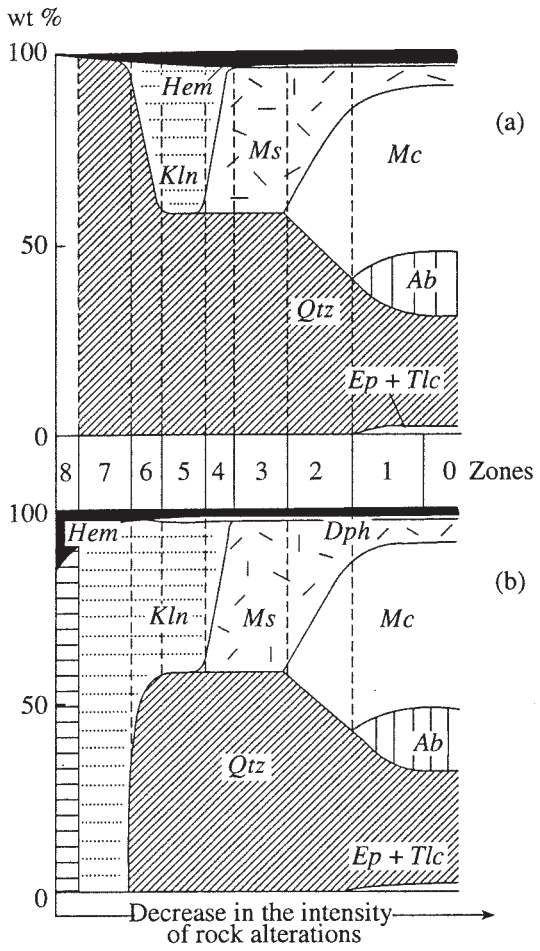

Fig. 2. Two principal types of zoning in the simulated argillization columns developing in granitic rocks.
(a) Column of the Si type that develops in liparite with solution 3/1 (H_2CO_3 = 1.0, HCl = 0.1, NaCl = 0.1, KCl = 0.01, and $CaCl_2$ = 0.01 mol/kg H_2O); (b) column of the Al type that develops in liparite with solution 30 (HCl = 0.0, other components as in 3/1); the thicknesses of both columns are chosen arbitrarily.

ride–carbonate solutions used in the simulations, the outer and intermediate zones (from zone 1 through 5 inclusive) of the metasomatic columns remained virtually the same in all models (Fig. 2).[3] Quartz–muscovite aggregates replaced albite in zone 1 and microcline in zone 2. Zone 3 had a quartz–muscovite composition (57–58 wt % *Qtz* + 36–37 wt % *Ms* + minor amounts of *Hem*, *Dph*, and *Crb*). In zone 4, the quartz content remained unchanged and muscovite was progressively replaced by kaolinite. Zone 5 consisted, in most columns, of a quartz–kaolinite aggregate (58 wt % *Qtz* + 34–36 wt % *Kln* + minor *Hem* and *Dph*). This zone was the last to show similarities in most columns, whose inner zones differed from model to model owing to distinct Al and Si behaviors.

Some solutions, for example, solution 3/1 (Fig. 2a), caused the replacement of kaolinite by quartz in the next zone (zone 6), then produced a monomineralic quartz zone (zone 7), and completely dissolved the rock (quartz) in zone 8.

Other solutions, for example 30 (Fig. 2b), caused gradual quartz dissolution in zone 6 under stable kaolinite, zone 7 was of nearly pure kaolinite composition, and zone 8 consisted of a diaspore aggregate (which contained, as in the kaolinite zone, subordinate amounts of *Hem* and *Dph*). Solutions 3/1 and 30 were different in that the former contained HCl (0.1 *m*), while no free strong acid was introduced into the latter; the concentrations of other components in the solutions were equal (Table 6).

Table 6 also reports the compositions of other solutions that produced argillisites of the Si and Al types in our models.

In the detailed analysis of dependences between the mineral assemblages in the rear zones of argillisites and the variations in the H_2CO_3 and HCl concentrations in the solutions that "reacted" with liparite, we carried out a series of calculations for "cross sections" with rock samples of constant mass. In some instances (Fig. 3), we calculated the results of interaction of each liparite sample with solutions containing constant concentrations of H_2CO_3 (1 *m*), NaCl (0.1 *m*), and KCl (0.01 *m*) at HCl concentrations decreasing from 10^{-1} to 10^{-6} *m*. In other series of simulations, (Fig. 4), each of the liparite samples of constant mass "reacted" with solutions having the same NaCl and KCl concentrations (0.1 *m* and 0.01 *m*, respectively) and variable concentrations of H_2CO_3 from 3.0 to 10^{-6} *m*.

Information in Figs. 3 and 4 can be read in different ways. Along the horizontal axis from left to right, changes are shown that take place in the mineral assemblages produced at the same $m_{rock}/m_{H_2O\ solution}$ ratios at systematically decreasing concentrations of HCl and H_2CO_3, which caused an increase in pH of the solution in equilibrium with the mineral assemblages (also from left to right).

Along the vertical axis upward, the zoning in the inner parts of the column is shown for the acid leaching of liparite (the "fracture wall" from which the solution starts to filter in the models is situated at the top) at any HCl and H_2CO_3 concentrations and under an increase in the $m_{rock}/m_{H_2O\ solution}$ ratio and the resultant increase in pH of the "filtrate."

For example, it follows from horizontal sections of Fig. 3 that, with the liparite mass used in the calculations (i.e., at $m_{rock}/m_{H_2O\ solution}$ ratios from 10^{-4} to 10^{-2}), all changes in the mineral assemblages are caused by variations in the HCl concentration in the solution only

[3] In contrast to the rule conventionally adopted for describing natural metasomatic rocks, in the text and Fig. 2, we assign consecutive numbers not only to stable but also to metastable (of transitional composition) zones, which correspond to the muscovite + kaolinite + solution and analogous fields in the phase diagrams.

Table 6. Composition (mol/kg H_2O) of solutions that caused the development of columns of Si and Al types

Solution composition	Si type								Al type							
	600	681	534	719	1*	3/1	53	54	24	24/0	24/1	D-1	10	12	30	3
H_2CO_3	0.2	1	1	1	1	1	0	1	e–6	e–6	0.01	0.1	1	1	1	0
HCl	0.1	0.1	0.1	–	0.1	0.1	0.1	0.1	e–6	e–3	e–6	–	e–3	–	–	–
NaCl	–	–	–	0.1	0.1	0.1	0.1	0.1	–	–	–	0.1	0.1	0.1	0.1	0.1
KCl	0.01	0.01	0.01	0.01	0.1	0.01	0.01	0.01	–	–	–	0.01	0.01	0.01	0.01	0.01
$CaCl_2$	0.01	0.01	0.01	0.01	–	0.01	0.01	0.01	–	–	–	0.1	–	–	0.01	0.1
H_2SO_4	–	–	–	0.01	–	–	–	–	–	–	–	–	–	e–3	–	–
Na_2SO_4	0.05	0.1	0.5	–	–	–	–	–	–	–	–	–	0.05	–	–	–
H_2S	–	–	–	–	–	–	0.01	0.1	–	–	–	0.01	–	–	–	0.1

* Numbers of solutions in the calculations.

within the range of 10^{-1} to 10^{-3} *m*, with lower HCl concentrations (at the specified constant concentrations of other components in the solutions) not affecting the composition and proportions of the newly formed phases.

As follows from vertical sections of Fig. 3, argillisites of the Si type are produced by chloride–carbonate solutions with HCl concentrations no lower than 5×10^{-3} *m*. The ordinate $\log m_{HCl} = -1$ corresponds to the column shown in Fig. 2a: the "zone" of complete dissolution of liparite near the fracture conduit gives way to a monomineralic quartz zone, which, in turn, is replaced by a quartz–kaolinite zone, and so on. At $\log m_{HCl} = -2$, the rear zone of the column is also characterized by the complete dissolution of quartz, but hematite remains stable. The subsequent zones are *Qtz*, *Qtz* + *Kln*, *Qtz* + *Ms*, etc. At HCl concentrations of $<10^{-3}$ *m* (and other conditions remaining the same), only Al-type argillization columns develop in liparite. They have a diaspore rear zone, which is followed by a monomineralic *Kln* zone and then by *Kln* + *Qtz*, *Qtz* + *Ms*, etc.

Horizontal "sections" of Fig. 4 show a decrease in the intensity of liparite alterations with decreasing CO_2 concentration in the solution. In fact, the horizontal "sections" are a part (variety) of acid leaching columns belonging to the Al type: *Dsp* ⟶ *Ms*, *Kln* ⟶ *Ms* ⟶ *Fsp*, *Ms* ⟶ *Fsp* (where *Fsp* is feldspars).

Vertical "sections" of Fig. 4 demonstrate that, under the conditions specified for the calculations, kaolinite develops in acid leaching columns in liparite under the effect of solutions containing from 3 to 0.01 *m* carbon dioxide; ordinates with these H_2CO_3 concentrations are characterized by complete argillization columns of Al type: *Dsp* ⟶ *Kln* ⟶ *Qtz* + *Kln* ⟶ *Qtz* + *Ms* ⟶ etc. At $m_{H_2CO_3} = 0.01$ *m*, the rear diaspore zones of the columns give way not to kaolinite zones but immediately to muscovite zones, which are then followed by quartz–muscovite zones, etc.

At still lower concentrations of dissolved CO_2, acid leaching columns in liparite (these columns cannot be ascribed to argillisites anymore) have a rear muscovite zone, which is followed by either a quartz–muscovite or a quartz-free feldspar–muscovite zone and, farther, by a quartz–feldspar–muscovite zone.

The appearance of albite or microcline in all of the model columns depends on the Na/K ratio in the solutions affecting liparite. At Na/K = 10 and low (10^{-6}) CO_2 concentrations in the solution (Fig. 4), albite is the first feldspar to appear in the columns (in fact, this mineral remains stable for a longer time). Solutions with Na/K = 1 produce columns in liparite in which the first feldspar to appear (or, more precisely, survive to farther inner zones) is microcline. A solution with $m_{NaCl} = m_{KCl} = 0.01$ and $m_{H_2CO_3} = 10^{-6}$ mol/kg H_2O produce the following metasomatic zoning: (0) liparite, (1) *Qtz* + *Mc* + *Ab* + *Ms* (plus, here and below, subordinate amounts of *Chl*, *Tlc*, *Ep*, *Dph*, and *Hem*), (2) *Qtz* + *Mc* + *Ms*, (3) *Mc* + *Ms*, (4) *Ms*. Solutions with $m_{NaCl} = m_{KCl} = 10^{-3}$ and $m_{H_2CO_3} = 10^{-6}$ give rise to somewhat different zoning: (0) liparite, (1) *Qtz* + *Mc* + *Ab* + *Ms*, (2) *Qtz* + *Mc* + *Ms*, (3) *Qtz* + *Ms*, (4) *Ms* (also with minor minerals in all zones).

Figure 4 also depicts another cause of the differences in the behavior of albite and microcline.[4] At a constant Na/K ratio equal to 10, albite is the first to appear in columns (survives to deeper inner zones) that are generated by solutions with $m_{H_2CO_3} < 5 \times 10^{-2}$ *m*. Higher concentrations of dissolved CO_2 ensure better preservation of microcline in argillisites (see also col-

[4] Here we do not touch upon another possible cause of the different behavior of albite and microcline, namely, the effect of the host rocks.

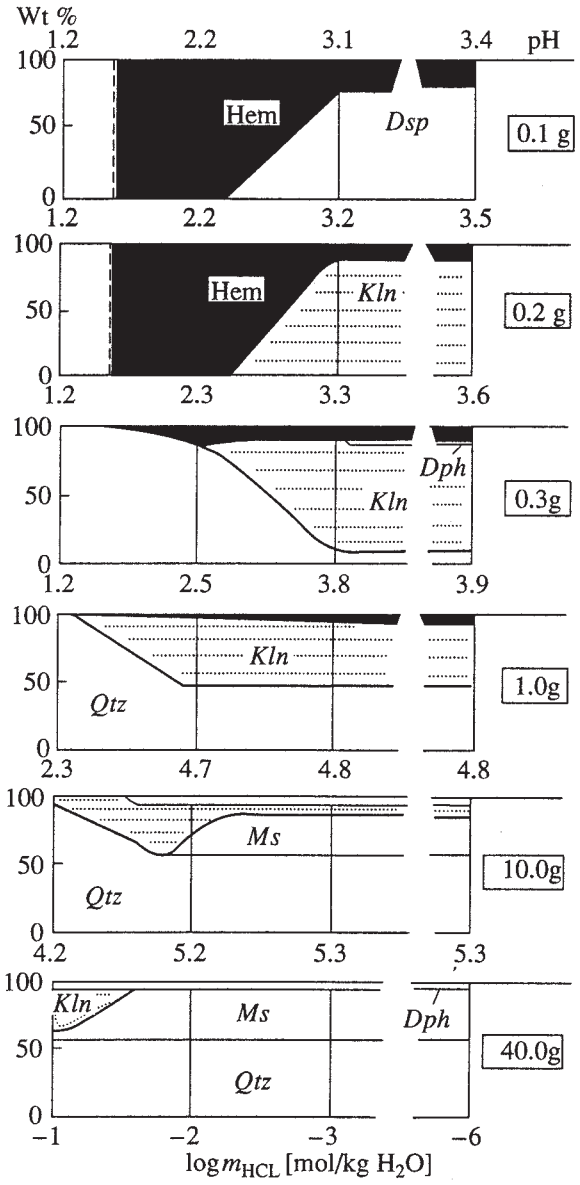

Fig. 3. Calculation of interactions between different "weights" of liparite (shown in boxes on the right-hand side) and 1 kg of an aqueous solution. The concentrations of H_2CO_3 (1.0), NaCl (0.1), and KCl (0.01) vary as the HCl concentration varies from 10^{-1} to 10^{-6} mol/kg H_2O; numerals above each column show the pH of the solutions in equilibrium with the newly formed solid phases or the association of solid phases (main ordinates); the system is open with respect to solution components.

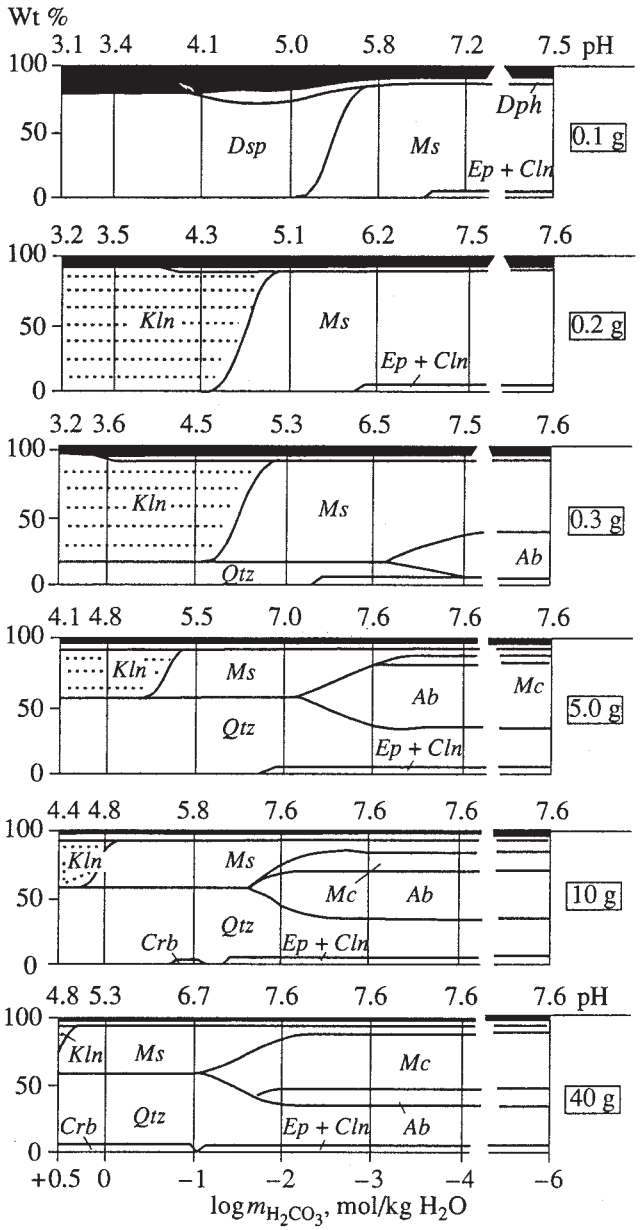

Fig. 4. Calculation of interactions between different "weights" of liparite (shown in boxes on the right-hand side) and 1 kg of an aqueous solution. The concentrations of NaCl (0.1) and KCl (0.01) vary as the H_2CO_3 concentration varies from 3.0 to 10^{-6} mol/kg H_2O; other conditions are the same as in Fig. 3.

umns in Fig. 2). Obviously, this problem deserves closer examination and explanation.

Discussion

Our models for metasomatic argillization columns developing in the same rock make it possible to analyze the causes of the different behaviors of Si and Al in the rear zones of these columns. A necessary prerequisite for the development of Si-type argillisites is not high or not low CO_2 concentrations in the solution reacting with the rock (as was proposed by Yu.V. Kazitsin) but the high acidity of these solutions. If this condition is not fulfilled, columns of the Al type are produced regardless of the CO_2 concentration in the solution.

There seems to be no correlation between the behavior of Si and Al during the origin of argillisites and the character of the strong acid that controls the pH of the

metasomatic solution. At m_{HCl} (or $m_{H_2SO_4}$) $< 5 \times 10^{-3}$ m, argillisites belong to the Al type and posses quartz-free rear zones (consisting of diaspore, kaolinite, or muscovite). At m_{HCl} (or $m_{H_2SO_4}$) $> 5 \times 10^{-3}$ m, monomineralic quartz zones of argillisites develop.

It follows from Figs. 3 and 4 that there can be combinations of conditions at which acid leaching in nature should results in columns deviating from the classic type. For instance, the absence of H_2S in the system can result in a monomineralic hematite rear zone of argillisites of the Si type. If the metasomatic solutions contain H_2S, particularly if its concentration is high (0.01–0.1 m), as in solutions 53 and 54 (Table 6), the reduction of Fe(III) of the liparite causes the development of a pyrite (but not hematite) rear zone of the column.

It is also possible that the kaolinite zone is absent from Al-type argillisites, whose rear diaspore zone (+ *Dph* + *Hem* or *Py*) gives way to a quartz-free muscovite zone (again + *Dph* + *Hem* or *Py*) and then to quartz–muscovite, etc. In columns of the Al type, the rear muscovite zone can be followed, first, by a quartz-free muscovite–feldspar (albite or microcline) zone and only after it by a feldspar–quartz–muscovite zone.

Of course, the deviations from the classic metasomatic zoning of acid leaching shown in Figs. 3 and 4 do not exhaust all variants possible in nature. Solutions introducing Mg or Fe and SO_4 or F into rocks can bring about other deviations from and complications of the classic zoning of acid leaching, including argillization columns.

Now consider the reactions that control the main mineral transformations in the rear zones of argillisites.

The quartz dissolution reaction

$$SiO_{2(cr)} + 2\,H_2O_{(liq)} = H_2SiO_{4(solution)}$$

is independent of pH. If a system of silica-free solution + rock has a small mass of rock, which cannot saturate the system in quartz, the latter component is fully dissolved, as can be seen for liparite samples of 0.1–0.2 g/kg H_2O and the pH of the equilibrium solution varying from 1.2 to 7.6.

The diaspore dissolution reaction

$$AlO(OH)_{(cr)} + 2H^+_{(solution)} = AlOH^{2+}_{(solution)} + H_2O_{(liq)}$$

is, conversely, controlled by the pH of the solution: the higher the H^+ ion activity, the more complete the diaspore dissolution. If the system has a constant mass of Al, which depends exclusively on the liparite mass in our calculations, and a low pH (0.1–0.3 g/kg H_2O and pH 2.3 in Fig. 3), the reaction can completely proceed to its right-hand side.

The reaction of kaolinite incongruent dissolution with the origin of quartz,

$$Al_4Si_4O_{18}H_{8(cr)} + 8H^+_{(solution)}$$
$$= 4SiO_{2(cr)} + 4AlOH^{2+}_{(solution)} + 6H_2O_{(liq)},$$

depends on the pH of the initial solution affecting kaolinite and, as the system becomes saturated with respect to quartz (at a liparite mass of ≤0.3 g/kg of solution and pH < 2.3), can result in the origin of a monomineralic quartz aggregate at the sacrifice of kaolinite.

The reaction of incongruent dissolution of kaolinite with the formation of diaspore,

$$Al_4Si_4O_{18}H_{8(cr)} + 6H_2O_{(liq)}$$
$$= 4AlO(OH)_{(cr)} + 4H_4SiO_{4(solution)},$$

does not depend on pH. Nevertheless, it actually proceeds at a pH higher than those determining the diaspore stability field, and if the solution is undersaturated with respect to quartz, the pH in the calculations is ≥2.3 and liparite mass is ≤0.1 g.

The reaction of muscovite replacement by diaspore,

$$KAl_3Si_4O_{12}H_{2(cr)} + H^+_{(solution)} + 6H_2O_{(liq)}$$
$$= 3AlO(OH)_{(cr)} + K^+_{(solution)} + 3\,H_4SiO_{4(solution)},$$

with a constant Si mass in the system (in the calculations, with a constant liparite mass) depends on the pH of the solution. The position of the boundaries of the diaspore and muscovite stability fields is also determined by the overall K mass in the system, which is controlled mostly by the KCl concentration in the initial solution if the rock mass is insignificant. This is realistic if the solution is undersaturated with respect to quartz.

The development of argillisites of Si and Al types can be envisioned as follows. As is well known, microfracturing and the related high permeability of the country rocks decreases away from the wall of macrofractures roughly hyperbolically. Because of this, regardless of whether the solutions spread perpendicular to the fracture or parallel to it, the maximum water content in the rock[5] should always be attained near the wall of any macrofracture (or near the selvages of a vein developing in it) and it rapidly decreases away from it.

Let us mentally subdivide the rock in which wall-rock metasomatics develop into thin layers parallel to the walls of the macrofracture that serves as a solution conduit. Let us assume that the multiply repeated circulation of the same ore-forming solution caused the interaction every 1 kg of it (or 1 kg of H_2O in it) with 0.1 g of the rock in layer 1, 0.2 g of rock in layer 2, an even a greater rock mass in layer 3, etc.

The initial highly acid solutions with m_{HCl} or $m_{H_2SO_4}$ = 0.1–0.01 m should cause the complete decomposition of the rock in the first two layers, because the solubility of Al-bearing phases at such low pH is very high and

[5] The final (integral) mass ratios of reacting rock and solution (m_{rock}/m_{H_2O} in solution) over a certain geological time span, for example, the ore stage of the hydrothermal process.

the solution is still not saturated with respect to quartz (the Si concentration in the solution remains twice as low as that in the equilibrium with quartz because of the low silica concentration in the system). Interaction between 0.3 g of liparite and 1 kg of acidic solution in layer 3 should result in the saturation of the solution with respect to quartz (2.41–2.35e–3 *m*), and a monomineralic quartz zone starts to develop.

If the solution affecting the rock is less acidic, the Al solubility in it is lower and the solution becomes saturated with respect to diaspore already within layer 1, with respect to kaolinite in layer 2, and only if the reacting rock mass is large enough (a large total mass of Si in the system), then the solution is saturated in quartz. Accordingly, the rear diaspore–kaolinite zone in the argillization column gives way to a zone of pure kaolinite and then to a quartz–kaolinite zone.

In nature, even at deposits with the same type of ore mineralization (for example, U–Mo), low- and medium-temperature wall-rock argillisites developing in similar rocks are characterized by different behaviors of Si and Al in the rear zones. The simulation of argillization process in liparite demonstrates that the factor responsible for these differences is the pH of the ore-forming hydrothermal solutions.

If the solution is highly acidic (m_{HCl} or $m_{H_2SO_4} \geq$ 0.005 mol/kg H_2O, regardless of the type of the strong acid), argillisites of the Si type develop, rear zone of which is monomineralic quartz or approaches this composition. The CO_2 concentration does not affect this process. If the hydrothermal solutions are less acidic, they produce argillisites of the Al type with a rear zone of kaolinite (dickite) or, sometimes, even diaspore (bohmite, bayerite) composition. A variety of these columns has a muscovite quartz-free rear zone.

2.3. Simulation of the General Regularities Controlling the Chemical Composition of Thermal Waters in Aluminosilicate Rocks

The previous sections of this publication were dedicated mostly to methodological approaches to determining the composition of solutions inducing certain types of alterations. However, there are some general regularities controlling the composition of aqueous (pore) solutions that can participate in the hydrothermal process. These regularities determine the composition of solutions by means of water–rock interactions and were closely considered in [Borisov, 1980; Borisov *et al.*, 1984, 1985c, 1988] and will be analyzed in this section.

System aluminosilicate rock–water

Interactions in the water–rock system belong to the most important processes that predetermine the chemical composition of natural waters. It is hardly probable that interactions of this type can occur in natural hydrochemical systems in the "pure" state, i.e., when the "solution" is pure water, because the chemistry of waters is controlled by a complex of processes, with an important role belonging to reactions with many volatile components (carbon dioxide, hydrogen sulfide, chlorides, etc.). Nevertheless, the results obtained on interactions between pure water and rocks make it possible to establish the fundamental relations between major components, i.e., a basis from which further variations in the composition of solutions (cold or thermal) start.

We examined interactions between aluminosilicate rocks of various compositions with pure water. The heterogeneous system H–O–Si–Al–Fe–Ca–Mg–Na–K is described by 40 phases of constant composition (minerals) and 27 aqueous solute species. As the eutonic (invariant) point is attained in a closed system, the maximum number of coexisting phases is equal to nine (eight minerals and a solution).

The thermodynamic calculations were conducted for 100, 200, and 300°C and the saturated water vapor pressure. Brought into contact with water were magmatic and metamorphic rocks (Table 7) that either represented the main crustal rock types (except sedimentary rocks) or had the highest, lowest, or average concentrations of certain major components.

The dependence of the solution composition on the rock/water ratio is a common feature of water–silicate systems, which is largely predetermined by the incongruent dissolution of most aluminosilicate minerals. Thus, as the rock dissolves, the water–rock system passes through a series of invariant states.

The rocks selected for modeling were "treated" with pure water at 12 different rock/water ratios (0.01–10000 g of the rock per 1000 g of H_2O) in a closed system. The calculations of equilibria with the increasing rock/water ratio imitate a systematic increase in the integral mass of rock involved in a reaction with the aqueous solutions filtrating through it. Equilibrium states at low ratios, before the eutonic point is achieved, represent the most altered portions of the rocks, with the number of equilibrium solid phases smaller than their maximum possible number. With an increase in the rock/water ratio, the alteration degree of the primary rocks decreases until equilibrium is attained between the aqueous phase and relatively weakly altered rocks, i.e., the origin of pore solutions. A further increase in the rock/water ratio does not result in any changes in the composition of the solution and minerals of the rock, because the solution is already saturated with respect to the latter. The pore solution composition can be assumed as equal to the solution composition at the eutonic point at a rock/water ratio equal to the corresponding rock porosity. However, the eutonic point is usually attained already at lower values of this ratio.

Table 8 summarizes the calculation results only for the solution compositions at eutonic points and mineral assemblages in equilibrium with them, as well as the

Table 7. Compositions (wt %) of rocks used in the models (after [Ronov and Yaroshevsky, 1976])

Oxide	*Cs*	*L*	*Grt*	*YGr*	*Kph*	*Mph*	*Ad*
SiO_2	61.13	72.80	72.41	66.15	61.51	67.66	59.59
Al_2O_3	17.03	13.49	14.27	15.45	17.37	14.30	17.31
K_2O	2.75	4.46	5.45	3.49	5.29	2.77	2.03
Na_2O	2.03	3.38	3.32	3.54	5.23	3.11	3.53
CaO	2.96	1.20	1.39	3.08	1.08	2.66	5.80
MgO	3.25	0.38	0.41	2.00	1.26	1.82	2.75
Fe_2O_3	2.68	1.45	0.87	1.74	1.92	1.24	3.33
FeO	4.26	0.88	3.75	2.70	3.35	3.75	3.13
H_2O	2.19	1.47	1.57	0.90	2.45	1.57	1.26

Oxide	*Ant*	*G*	*Aph*	*Tb*	*B*	*D*
SiO_2	50.40	48.28	52.01	49.46	49.06	40.44
Al_2O_3	28.30	17.88	14.21	15.51	15.70	0.86
K_2O	0.74	0.89	0.84	0.23	1.52	0.04
Na_2O	3.67	2.55	2.47	2.68	3.11	0.10
CaO	12.46	10.99	9.35	11.24	8.95	0.70
MgO	1.25	7.51	7.13	7.90	6.17	46.32
Fe_2O_3	1.06	3.16	2.59	2.46	5.38	2.84
FeO	1.12	5.95	8.11	7.97	6.37	5.54
H_2O	0.75	1.45	1.53	0.69	1.62	2.88

Note: Here and in table 8, the following symbols are used to denote rocks: *Cs*—paragneisses and crystalline schists, *L*—liparite, *Grt*— granite, *YGr*—average composition of the Earth's granitic layer, *Kph*—keratophyre, *Mph*—metamorphosed acid volcanics, *Ad*—andesite, *Ant*—anorthosite, *G*— gabbro, *Aph*—amphibolites and metamorphosed mafic rocks, *Tb*—tholeiitic basalt, *B*—basalt, *D*—dunite.

rock/water ratios at which the equilibria are attained. As this ratio increases from 0.00001 to the value corresponding to the invariant point, the Na and Si concentrations in equilibrium solutions increase for virtually all rocks, while the Ca and Mg concentrations decrease, and those of K, Fe, and Al behave differently depending on the primary rock composition and the newly formed assemblages of secondary minerals. The pH of the solution increases. The ratios of concentrations in the K/Na, Ca/Mg, and Al/Si pairs in the solutions at eutonic points vary relatively little. These data indicate that the main factor controlling the composition of the equilibrium aqueous solution, its pH, and Eh is the chemical type of the rock.

The solutions interacting with acid rocks have the lowest pH, are less concentrated, and are characterized by weakly reducing properties (the lowest equilibrium partial pressures of hydrogen). The solution composition is stabilized already at relatively low rock/water ratios. The typical minerals of the equilibrium phase assemblage are quartz, muscovite, potassium feldspar, hydromicas, calcium aluminosilicates, chlorites, and albite.

The solutions that interacted with basic rocks have higher pH, are more concentrated, and act as strong reducers (reactions with these rocks create high partial pressures of hydrogen). The composition of the solutions is stabilized at higher rock/water ratios; because of this eutonic points of the solutions interacting with basic rocks are attained over longer time spans (at equal other conditions) than for solutions interacting with acid rocks. The equilibrium mineral assemblages include albite, chlorite, epidote, hydromicas, muscovite, and Ca aluminosilicates.

Over the interval of rock/water ratios in question, ultrabasic and alkaline rocks are decomposed by water (no invariant point is attained).

It is worth noting an important geochemical implication of our simulations: an increase in the hydrogen concentration in the solutions interacting with basic and ultrabasic rocks. An increase in the hydrogen concentration of natural thermal waters in areas of modern magmatism with such rocks was documented by Kononov [1983] and was then discussed from various geochemical standpoints. It is commonly thought that the hydrogen is of endogenic provenance. However, the results of physicochemical simulations indicate that high hydrogen partial pressures can result from high-temperature interactions between water and basic rocks. For example, thermodynamic simulations carried out by Grichuk *et al.* [1985] and Dmitriev *et al.* [1999] have established that reactions between seawa-

Table 8. Composition (mg/l) of aqueous solutions at the invariant point (closed system)

Rock	*Cs*	*L*	*Grt*	*YGr*	*Kph*	*Mph*	*Ad*	*Ant*	*G*	*Aph*	*Tb*	*B*	*D*
						100°C							
Equilibrium minerals/components	1, 3, 7, 8, 10, 23, 26, 31	1, 3, 7, 8, 10, 23, 26, 31	1, 2, 3, 7, 10, 23, 26, 31	1, 2, 3, 7, 10, 23, 26, 31	1, 2, 7, 10, 19, 23, 26, 31	1, 2, 7, 10, 19, 23, 26, 31	3, 7, 10, 12, 17, 19, 23, 31	3, 7, 10, 12, 17, 19, 23, 40	–	7, 10, 13, 17, 18, 19, 23, 31	7, 10, 12, 13, 17, 19, 23, 40	–	2, 6, 19, 23, 24, 27*
pH	8.974	8.974	9.715	9.715	10.00	10.00	10.21	10.26	–	10.67	10.73	–	11.66
K	5.07e–1	5.07e–1	3.0	3.0	6.24	6.24	5.07	5.85	–	25.0	23.8	–	1440
Na	322	322	193	193	391	391	345	368	–	1610	1560	–	11800
Ca	2.72e–7	2.72e–7	1.20e–5	1.20e–5	5.60e–5	5.60e–5	2.04e–4	1.88e–4	–	3.44e–3	5.20e–3	–	1.16
Mg	6.24e–5	6.24e–5	5.52e–6	5.52e–6	2.64e–6	2.64e–6	2.64e–6	6.48e–6	–	1.37e–7	2.88e–7	–	8.88e–4
Al	1.97e–1	1.97e–1	3.78e–2	3.78e–2	2.00e–2	2.00e–2	1.86	2.21	–	5.94e–2	7.02e–1	–	1.92e–1
Si	56	56	174	174	33.6	33.6	115	120	–	728	504	–	4.20
Fe(II)	8.40e–7	8.40e–7	1.12e–4	1.12e–4	8.40e–4	8.40e–4	4.76e–5	5.32e–5	–	1.12e–2	2.35e–3	–	42.6
Fe(III)	1.18e–1	1.18e–1	1.18e–3	1.18e–3	6.16e–4	6.16e–4	1.23e–3	1.23e–3	–	3.86e–4	1.06e–5	–	7.84e–5
P_{H2}	1.4e–10	1.4e–10	1.3e–7	1.3e–7	6.7e–6	6.7e–6	2.4e–9	2.4e–9	–	5.1e–5	6.3e–3	–	1.4e–9
Rock/water	0.01	0.01	0.04	0.04	0.4	0.4	0.4	0.4	–	0.4	0.4	–	5
						300°C							
Equilibrium minerals/components	1, 3, 8, 10, 17, 19, 23, 26	1, 7, 8, 10, 17, 19, 23, 31	1, 7, 8, 10, 17, 19, 23, 31	1, 7, 8, 10, 17, 19, 23, 31	1, 7, 8, 10, 17, 19, 23, 31	1, 7, 8, 10, 17, 19, 23, 31	1, 7, 8, 10, 17, 19, 23, 31	8, 10, 12, 17, 19, 20, 23, 38	8, 10, 12, 17, 19, 20, 23, 38	1, 7, 10, 13, 17, 19, 23, 31	7, 10, 13, 17, 19, 20, 23, 38	2, 7, 10, 17, 19, 23, 24, 30	2, 6, 24, 25, 27*
pH	7.742	7.752	7.752	7.752	7.752	7.752	7.752	8.503	8.503	8.260	9.394	10.08	10.21
K	5.46	5.85	5.85	5.85	5.85	5.85	5.85	13.6	13.6	12.9	18.7	1330	140
Na	21.4	21.6	21.6	21.6	21.6	21.6	21.6	163	163	50.6	897	8050	11600
Ca	8.80e–5	8.80e–5	8.80e–5	8.80e–5	8.80e–5	8.80e–5	8.80e–5	9.20e–4	9.20e–4	2.16e–3	1.44e–3	5.60e–4	1.52e–2
Mg	2.30e–4	2.21e–4	2.21e–4	2.21e–4	2.21e–4	2.21e–4	2.21e–4	7.92e–5	7.92e–5	1.22e–5	1.22e–5	6.48e–6	2.28e–3
Al	11.3	11.3	11.3	11.3	11.3	11.3	11.3	124	124	5.40	270	432	70.2
Si	308	308	308	308	308	308	308	95.2	95.2	336	143	476	5.88
Fe(II)	3.81e–4	4.03e–4	4.03e–4	4.03e–4	4.03e–4	4.03e–4	4.03e–4	2.30e–3	2.30e–3	7.84e–3	1.18e–1	4.54	78.4
Fe(III)	95.2	95.2	95.2	95.2	95.2	95.2	95.2	5.60e–1	5.60e–1	6.72e–1	6.16e–1	26.9	7.84
P_{H2}	1.1e–5	1.0e–4	1.0e–4	1.0e–4	1.0e–4	1.0e–4	1.0e–4	0.41	0.41	12	13.5	0.28	63
Rock/water	0.04	0.01	0.01	0.01	0.01	0.01	0.01	0.4	0.4	0.5	0.8	10	5

Note: Solid phases: (1) quartz, (2) magnetite, (3) hematite, (4) diaspore, (6) brucite, (7) microcline, (8) muscovite, (10) albite, (11) paragonite, (12) lawsonite, (13) wollastonite, (17) epidote, (18) Fe-tremolite, (19) tremolite, (20) pargasite, (23) Fe-chlorite, (24) phlogopite, (25) Mg-chlorite, (26) talc, (27) serpentine, (31) heulandite, (38) prehnite, (40) analcime, * invariant point is not attained.

ter and tholeiitic basalts at temperatures of 300–350°C can give rise to hydrogen concentrations as high as 0.025 mol/1000 g H_2O.

A factor that can directly control Eh is the Fe^{2+}/Fe^{3+} ratio in the assemblages of secondary minerals that develop after the primary rocks. The reducing composition of solutions that react with basic and ultrabasic rocks, for instance, the high hydrogen concentrations identified in our simulations, is caused by the Fe^{2+}–Fe^{3+} redox pair and its interaction with water.

Comparison of the calculated concentrations of elements and their actual contents in thermal groundwaters

During the first stage of our research, we examined only the simplest situations when pure water interacts with primary intrusive and volcanic rocks. Natural analogues of such simple systems are rare, but they do exist. These are, for example, nitrogen-bearing thermal waters that occur in intrusive and volcanic rocks in areas of Alpine epiplatform orogenesis. The thermal waters are weakly mineralized and are produced by direct phase interactions between intrusive (or volcanic) rocks and waters at elevated temperatures, virtually without chlorides and carbon dioxide involved. The gas components of these thermal waters are strongly dominated by nitrogen (up to 90–99%). Nitrogenous thermal waters can have temperatures as high as 100°C or more and are characterized by the following geochemical features: their overall mineralization does not exceed 1 g/l; their chemical composition varies from H_3SiO_4–Na and HCO_3–Na to SO_4–Na, and pH ranges from 7 to 9.5; and their gas constituents can be, along with nitrogen, O_2, CH_4, and rare gases.

According to these chemical properties of nitrogenous thermal waters, they are the most convenient waters to compare with the simulation results. There are two important points that should be preliminarily mentioned, because they determine the capabilities and interpretation principles of our analysis.

In the calculations, we ignored carbonate, sulfide–sulfate, and other equilibria that affect the Ca and Mg distribution in natural thermal waters. Because of this, our models cannot be fully adequate for natural processes with respect to these elements. This made it impossible to compare the calculated and actual Ca and Mg concentrations. We were left with the possibility of comparing only the Na and K concentrations, which depend not as strongly on carbonate and other equilibria ignored in our models but are controlled by the direct interaction of waters with aluminosilicate minerals.

In comparing the calculated and actual Na and K concentrations, it is possible to deal only with the orders of magnitude of the concentrations of these elements, the tendencies in their distribution, and constraints, because the different velocities and filtration

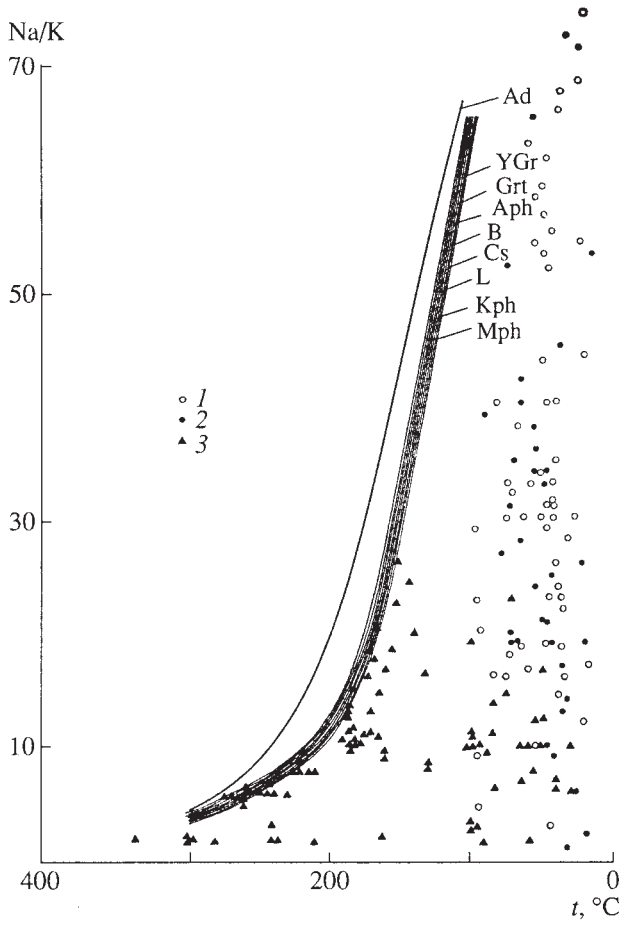

Fig. 5. Comparison of the Na/K ratios obtained by simulating water–rock interactions (closely spaced lines) and those observed in nitrogen- and carbon dioxide-bearing thermal waters in massifs of crystalline rocks. Waters: (*1*) nitrogen-bearing [Lomonosov, 1974; Kononov, 1983; S.R. Kraynov, personal communication]; (*2*) nitrogen-bearing [Borov and Daiyski, 1959; Kusitaseva and Melamed, 1959); (*3*) carbon dioxide-bearing [Kononov, 1983; Ellis, 1970; Pampura, 1977]. See Table 7 for explanations of the rock symbols near the lines.

times of groundwaters in rocks cause different disequilibration degrees of discrete portions of a water–rock system or different rock/water ratios during their interactions.

The calculated concentrations of Na during high-temperature interactions between water and various intrusive and volcanic rocks are from $n \times 10$ to $n \times 100$ mg/l at maximum values on the order of 340–370 mg/l (Table 8). These values are roughly the same as the most common Na concentrations documented in nitrogenous thermal waters (Fig. 5).

The equilibrium K concentrations in the solutions interacting with aluminosilicate rocks are usually a few mg/l at maximum concentrations of approximately 25 mg/l (Table 8). These values are commensurable with the K concentrations determined in natural ther-

Table 9. Equilibrium concentrations (mg/l) of elements in solutions interacting with a rock at different partial pressures of CO_2

T, °C	P_{CO_2}	Na	K	Mg	Ca	Al	Si	C	pH
Granitic rock + H_2O + P_{CO_2} (atm)									
25	1e–3.4	1170	0.355	1.51e–3	9.20e–2	3.51e–3	10.9	504	9.62
50	1e–3	2530	1.05	2.28e–4	3.16e–2	2.97e–2	30.8	960	9.59
100	1e–2	1770	6.63	8.64e–5	2.96e–2	1.73e–1	58.8	816	9.01
150	1e–1.5	2230	16.0	1.15e–5	1.08e–2	1.08	132.0	864	8.95
Granitic rock + H_2O (solution with $m_{HCl} = 0.9$) + P_{CO_2} (atm)									
25	1e–3.4	2180	6.63	1.18	64.0	3.51e–4	5.88	33.6	8.45
50	1e–3	2210	8.97	2.40e–2	3.72	5.67e–3	14.6	144	8.79
100	1e–2	2210	85.8	1.61e–2	8.0	2.70e–2	33.6	104	8.1
150	1e–1.5	2230	117.0	1.75e–3	2.24	2.19e–1	75.6	144	8.15

Note: The equilibrium assemblage of solid phases includes quartz, Mg-silicate, K-mica, Na-mica, $CaCO_3$, and Ca-aluminosilicate.

mal waters. At the same time, the Na and K concentrations in natural thermal waters are usually lower than our calculated values. This is explained by the fact that the calculated data pertain to eutonic points and correspond to the highest possible concentrations that are formed in the system water–aluminosilicate rock if the latter has time to adjust to the chemically equilibrated state.

The similarities between the calculated and actual concentrations of Na and K concentrations in nitrogenous thermal waters are reflected in the fact that the observed Na/K ratios are also constrained from above by the calculated equilibrium values (Fig. 5). It is also worth mentioning that naturally occurring and calculated concentrations are close or coincide at high temperatures, which seems to be explained by the high rates of heterogeneous reactions. Natural thermal waters show the same general temperature dependences of the Na/K ratio that were established in the physicochemical simulations. Moreover, further geochemical analysis of the distribution of the Na/K ratio in various types of thermal waters (not only nitrogenous) indicates that the calculated values mark the limit of the Na/K ratios in most geochemical types of thermal waters in equilibrium with aluminosilicate rocks. This is explained by the fact that the Na/K ratio in thermal waters during their interaction with aluminosilicate rocks is affected relatively little by carbonate and other equilibria. Consequently, the Na/K ratios even in carbonate thermal waters with high concentrations of CO_2, Cl, Na, and K are close to the calculated values. As can be seen from Fig. 5, the fields of the Na/K ratio in nitrogenous and carbonaceous thermal waters are limited by the equilibrium lines calculated for solutions interacting with various types of aluminosilicate rocks.

The above comparison illustrates the potentialities of physicochemical simulations, a technique that makes it possible to employ even relatively simple models to predict geochemical phenomena taking place in natural systems of rocks and groundwaters. It should be emphasized that our modeling definitely indicates that the composition of the equilibrium aqueous solution, its pH, and Eh are controlled by the chemical type of the rock (for example, acid or basic), not simply by variations in the concentrations of certain chemical elements in it.

Role of volatile components in the aluminosilicate rock–water system

Now let us examine the interactions of an aqueous solution containing CO_2 and chlorides with an aluminosilicate rock of granitic composition (we assumed the average composition of the granitic layer of the continental crust).

The introduction of other components into the system results in changes in the solution composition and the equilibrium phase assemblage. For example, if the system contains CO_2 (acidic component), the solution in equilibrium with the solid phase becomes less alkaline, and, correspondingly, the concentrations of species typical of alkaline environments decrease. At the same time, solute species form complexes with CO_2 and Cl and thus increase the concentrations of elements associated with volatile components (these are mostly alkalis and alkali earths).

It follows from Tables 8 and 9 that the introduction of CO_2 into the granite–water system leads to solution acidification, disappearance of feldspars from, and appearance of calcite in the equilibrium mineral assemblage. The concentrations of elements in the solution vary accordingly to their complexation. If Cl is intro-

Table 10. Equilibrium concentrations (mg/l) of components in solutions interacting with a granitic rock at different temperatures, rock/water ratios, and partial pressures of CO_2

g of rock per kg of H_2O	Na	K	Mg	Ca	Al	Si	HCO_3	pH
25°C, $P_{CO_2} = 10^{-3.4}$ atm								
0.001	2.2e–2	2.6e–2	1.3e–2	5.2e–2	3.0e–6	0.3	1.0	5.90
0.01	0.2	0.3	0.1	0.2	4.9e–5	3.1	3.0	6.83
0.1	2.2	1.8	1.3	2.5	1.1e–4	5.9	23.0	7.78
0.4	9.0	0.8	0.5	8.0	2.3e–4	5.9	51.0	8.14
1.0	22.3	0.9	0.2	5.6	2.7e–4	6.2	78.00	8.30
4.0	89.7	2.1	3.4e–2	2.4	4.6e–4	6.4	234.0	8.66
10	223.1	1.0	8.9e–3	0.6	1.0e–3	7.3	540.0	9.10
100	1541.0	0.5	1.2e–3	7.2e–2	3.8e–3	12.0	3120.0	9.68
4000	72680.0	21.1	1.8e–4	7.2e–3	5.7e–3	53.2	116400.0	10.44
50°C, $P_{CO_2} = 10^{-3}$ atm								
0.001	2.2e–2	2.6e–2	1.3e–2	2.5e–2	2.7e–4	0.3	1.5	5.71
0.01	0.2	0.3	0.1	0.2	3.0e–4	3.08	3.5	6.58
0.1	2.2	2.1	0.7	2.5	7.0e–4	11.2	21.0	7.49
0.4	9.0	1.2	0.2	3.7	1.2e–3	11.2	37.0	7.75
1.0	22.3	2.6	6.7e–2	2.8	1.4e–3	11.5	72.0	8.03
4.0	89.7	0.9	7.7e–3	1.6	2.0e–3	12.6	240.0	8.54
100	231.0	1.1	2.4e–4	3.6e–2	2.6e–2	47.6	4500.0	9.56
200	299.0	1.2	2.0e–4	2.8e–2	3.0e–2	33.6	6000.0	9.63
4000	7268.0	28.5	5.3e–5	5.2e–4	4.1e–2	134.4	120600.0	10.23

duced into the system, the concentrations of alkalis and alkali earths increase, whereas the concentrations of Si and Al decrease because of a decrease in the solution alkalinity (Table 9).

Table 10 lists data on the variations in the concentrations of elements in the system granite–aqueous solution under a CO_2 pressure depending on the rock/water ratio. Data on the system basalt–aqueous solutions were reported by Ryzhenko *et al.* [1977, 2000], Kraynov and Ryzhenko [2000], and Ryzhenko and Kraynov [2002]. The aqueous phase is progressively enriched in all elements as the rock/water ratio increases. However, as the solution becomes saturated with respect of an ever growing number of solid phases, the behaviors of elements become different.

The aqueous phase composition in the granite–solution system was calculated for different chloride concentrations in the initial solution. The solution was assumed to contain chloride, hydrocarbonate, carbonate, sulfate, and hydrosulfide complex species. Table 11 reports the concentrations of elements in the solution in equilibrium with granite at variable rock/water ratios, containing 350 mg/l Cl and occurring under CO_2, H_2, and H_2S partial pressures ($P_{H_2} = 10^{-20.8}$ atm at 25°C and $10^{-18.9}$ atm at 50°C, $P_{H_2S} = 10^{-25}$ atm) at temperatures of 25 and 50°C. The value of P_{H_2} was selected in such a way as to maintain the redox potential of the solution at $P_{O_2} = P_{H_2}$. The value of P_{H_2S} was specified so that the sulfate sulfur concentration at a given Eh value corresponded to the values typical of natural waters.

The main effect of the introduction of volatiles (CO_2, Cl, etc.) into the system aluminosilicates–water was the extraction of alkalis and alkali earths from the rock proportionally to the introduced massed of volatiles and the corresponding changes in the rock composition.

Discussion of modeling results

Our simulation results can be assayed qualitatively and quantitatively, i.e., from the viewpoint of their general comparison with known geochemical regularities governing the chemical composition of groundwaters, as well as their correlation with variations in the actual concentrations of certain elements in groundwaters.

The simulation results can be qualitatively assessed from the standpoint of general problems in the origin of the chemical composition of groundwaters in granitic rocks.

Table 11. Equilibrium concentrations (mg/l) of components in solution containing 350 mg/l Cl and interacting with a granitic rock at different temperatures, and partial pressures of CO_2

g of rock per kg of H_2O	Na	K	Mg	Ca	Al	Si	SO_4	HCO_3	pH
25°C, $P_{CO_2} = 10^{-3.4}$ Pa									
4	62.1	54.6	10.3	100.0	2.3e–5	5.9	5.7e–3	2.0	6.37
10	142.6	9.0	3.8e–4	92.0	6.5e–6	5.9	11.4	44.5	8.02
40	575	1.5	1.9e–6	3.6	6.5e–6	6.7	461	300	8.82
200	2530	0.8	2.2e–7	5.6	6.5e–6	8.1	3360	840	9.19
400	3910	1.2	1.5e–7	1.5	5.4e–6	8.4	6720	1260	9.27
1000	30350	3.2	7.7e–8	1.3	3.8e–6	9.8	18240	2280	9.42
2000	21620	7.0	5.0e–8	1.2	2.7e–6	10.9	40320	3900	9.51
10000	40300	46.8	1.8e–8	1.0	1.5e–6	14.8	26880	19200	9.72
50°C, $P_{CO_2} = 10^{-3}$ Pa									
4	62.1	66.3	7.4	100.0	1.2e–4	11.2	3.3	6.5e–2	6.04
18	142.6	46.8	3.1e–4	64.0	2.6e–5	11.2	63.3	0.3	7.72
20	276	15.2	6.2e–6	4.8	2.3e–5	12.0	259	4.0	8.35
1000	15180	17.9	1.6e–6	22.8	2.4e–5	13.2	826	19200	8.53
2000	32890	16.4	8.6e–7	21.2	2.4e–5	13.4	1340	42000	8.62
4000	48760	22.2	6.7e–7	20.4	2.2e–5	13.7	1820	62400	8.66

(1) Water interaction with granite (in a system open with respect to CO_2 and H_2S) results in solutions enriched in Na. The general trend in the variations of the solution chemistry with increasing rock/water ratios and temperature is as follows:

$$HCO_3\text{–}Na\text{–}Ca\text{–}Mg \longrightarrow HCO_3\text{–}Na\text{–}Ca$$

$$\longrightarrow HCO_3\text{–}Na \longrightarrow HCO_3\text{–}SO_4\text{–}Na \longrightarrow SO_4\text{–}Na$$

The cationic composition of the solutions of this series is formed in relation with an increase in the Na concentration at an increasing rock/water ratio, decreasing Ca concentration, and increasing temperature.

(2) An increase in the Cl concentration in the initial solutions intensifies Na and Ca transfer from the rocks into aqueous solution. The higher the Cl concentration and the stronger chloride complexes of the elements (Ca > Na > K) the stronger the increase in the concentration of major elements. The process is intensified with increasing temperature.

(3) The effects of temperature, rock/water ratio, and the chloride concentration on the chemical composition of the solutions are similar in several respects. These parameters can be interchangeable relative to a number of factors, and an analogous geochemical effect can be achieved at a lower rock/water ratio but a higher temperature. Conversely, at a higher rock/water ratio, an analogous chemical composition can be formed at a lower temperature; i.e., stronger rock reworking is equivalent to the action of a higher temperature.

Analogously, a higher chloride concentration in the initial solution exerts an effect on the final solution composition equivalent to the effect of a higher rock/water ratio and temperature. At a higher chloride concentration in the initial solution, analogous rock recycling and Na and Ca extraction from it is achieved at a lower rock/water ratio and temperature.

These conclusions are in agreement with known geochemical regularities controlling the composition of cold and thermal waters in granitoid rocks and with general compositional characteristics of these waters. In particular, the results obtained on nitrogenous thermal waters in areas of epiplatform orogenesis indicate that an increase in the origin depths of the waters, i.e., an increase in the temperature and the rock/water ratio, is correlated with systematic changes in their geochemical types in the succession

$$HCO_3\text{–}Ca \longrightarrow HCO_3\text{–}Ca\text{–}Na \longrightarrow HCO_3\text{–}Na\text{–}Ca$$

$$\longrightarrow HCO_3\text{–}Na \longrightarrow HCO_3\text{–}SO_4\text{–}Na \longrightarrow SO_4\text{–}Na$$

which is analogous to that obtained by simulating interactions in the granite–water system.

It is also known that, regardless of the source of Cl, an increase in the Cl concentration in nitrogenous thermal waters in massifs of crystalline rocks leads to an increase in the mineralization owing to an increase in the Na and, particularly, Ca concentrations (nitrogenous thermal waters of the Issyk Kul' group: Kyzyl Su, Altyn Arasan, and others).

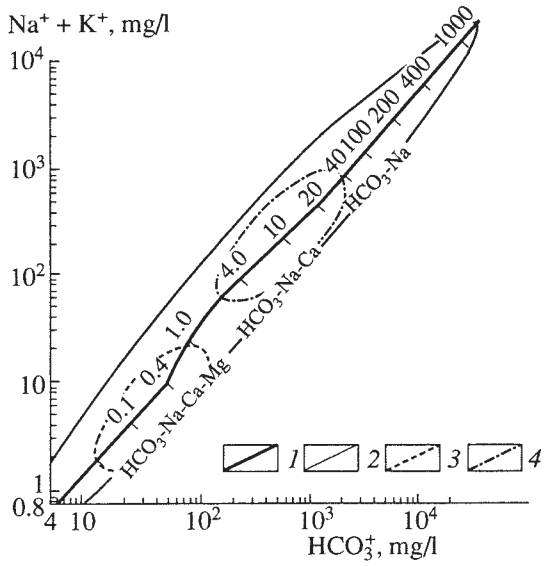

Fig. 6. Calculated and observed concentrations of components in the system HCO_3^-–($Na^+ + K^+$). (*1*) Calculated equilibrium concentrations of the components in solutions interacting with a granitic rock. Shown on the line are the changes in the geochemical types of the resulting solutions and the rock/water ratios assumed in the calculations (25°C, $P_{CO_2} = 10^{-3.4}$ atm). The fields of the actual distributions of HCO_3^- and $Na^+ + K^+$ in waters interacting with the following rocks: (*2*) Lovozero and Khibina massifs of alkaline rocks, (*3*) massifs of ultramafic rocks in the Kola Peninsula; (*4*) massifs of granitoid rocks in the arid zone of Middle Asia.

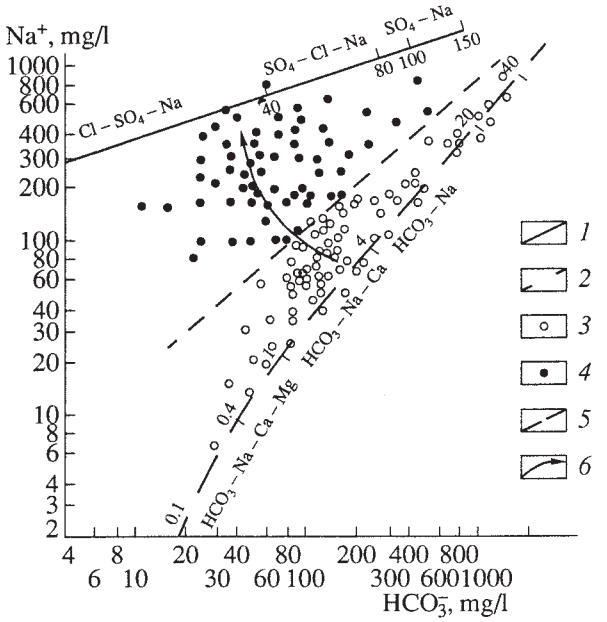

Fig. 7. Calculated and observed concentrations of components in an HCO_3^- vs. Na^+ diagram. (*1*) Calculated equilibrium concentrations of components in a solution containing 350 mg/l Cl and interacting with a rock of granitic composition (50°C, $P_{CO_2} = 10^{-3}$, $P_{H_2} = 10^{-18.9}$, $P_{H_2S} = 10^{-25}$ atm); (*2*) calculated equilibrium concentrations of components in solution interacting with granite (50°C, $P_{CO_2} = 10^{-3}$); (*3*, *4*) measured concentrations of components in thermal waters in massifs of crystalline rocks in the territory of the former Soviet Union and Bulgaria: (*3*) HCO_3–Na waters with temperatures of 20–80°C; (*4*) SO_4 (Cl)–Na waters with temperatures of >50°C; (*5*) boundary between thermal waters of HCO_3–Na and SO_4(Cl)–Na compositions (at specified temperatures); (*6*) direction in which the temperature and SO_4^{2-} concentration of thermal waters increase. Shown on lines are the changes in the geochemical types of the resulting solutions and the rock/water ratios assumed in the calculations.

Hence, the analysis of our physicochemical simulation results obtained on the granite–water system qualitatively demonstrates that these results fairly adequately reflect principal regularities controlling the chemistry of groundwaters in crystalline rocks.

For example, our simulation results can be compared with the actual distributions of elements in groundwaters formed in crystalline rocks. There are extensive data on the chemistry of free-aquifer cold groundwaters in massifs of intrusive rocks of acid and alkaline composition and the chemistry of confined-aquifer thermal (30–100°C) waters produced in granitoid massifs in areas of epiplatform orogenesis (Tien Shan, Pamirs, Rhodope Mountains, Balkans, and Primor'e in the Russian far East). The calculated and actual concentrations of elements at low (25°C) temperatures can be compared only for waters of the HCO_3–Na type, while the analogous figures for high (50–100°C) temperatures can also be correlated for the SO_4–HCO_3–Na and SO_4–Na types. The results of comparison between the calculated and actual concentrations in groundwaters produced in acidic and alkaline intrusive rocks are demonstrated in Figs. 6 and 7 and imply the following conclusions:

* The closeness between the calculated and measured concentrations depends on the temperature, geochemical properties of the elements, and the rock/water ratio.

* The higher the temperature, the closer the actual concentrations to the calculated ones. This pertains first of all to simple Na–HCO_3 systems, whose compounds are more soluble, and their solubility increases with temperature. Finally, according to the aforesaid about the similarities between the effects exerted by temperature and the rock/water ratio, the actual concentrations of elements in groundwaters approach the calculated values with increasing temperature as they also should do with an increase in the rock/water ratio.

The aforesaid does not mean that our simulation results are always in good agreement with the actual

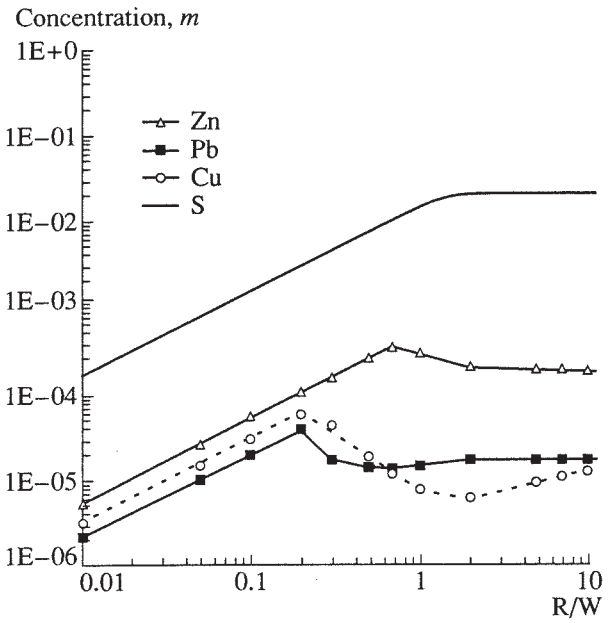

Fig. 8. Variations in the concentrations of ore elements and sulfide sulfur depending on variations in the rock/water ratio (R/W) in the granite–solution system (370°C, 1 kbar). Plotted on the ordinate are the bulk concentrations of components (logarithmic scale); plotted on the abscissa is the rock/water ratio (logarithmic scale).

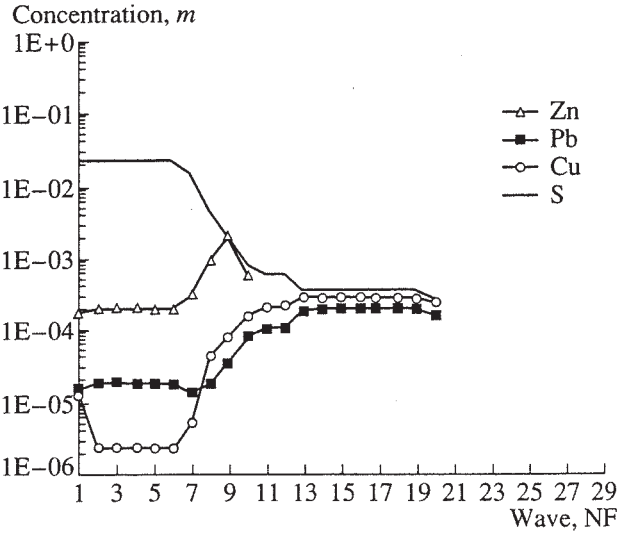

Fig. 9. Variations in the concentrations of ore elements and sulfide sulfur in the equilibrium solution after multiple interactions between granite and the primary fluid (370°C, 1 kbar). Plotted on the ordinate are the bulk concentrations of components (logarithmic scale); plotted on the abscissa are the numbers of waves (portions) of interaction (NF).

concentrations of elements in groundwaters. For instance, the assumed low-sulfate model for the chemical composition of groundwaters in granites predetermines significant discrepancies between the calculated and actual Mg concentrations in groundwaters: the latter are one order of magnitude higher than the former.

In recent years this research was continued by other researches [Kraynov and Ryzhenko, 2000; Ryzhenko *et al.*, 2000; Ryzhenko and Kraynov, 2002].

2.4. Estimation of the Ore Potential of Hydrothermal Solutions

The data reported in Sections 2.1–2.3 pertain only to the main components of natural solutions and to major elements. We still have not touched upon the techniques for estimating the concentrations of minor (including ore-forming) elements in a hydrothermal solution. This issue is closely related to the problem of the source of ore components. We will consider one of the possible solution variants within the framework of the latter problem [Borisov *et al.*, 1995; Borisov and Shvarov, 1995, 1996, 1998].

In simulating the processes responsible for the origin of vein Pb–Zn deposits, we assumed the working hypothesis that the initial ore-forming solution is produced in the root portions of the deposits by means of mobilizing ore components during reaction between the primary hydrothermal solution and country granites (this problem is discussed in detail in Chapters 5 and 6).

The granite–fluid system is described by 15 independent components: H–O–K–Na–Ca–Mg–Al–Si–Fe–C–Cl–S–Zn–Pb–Cu. The model for the aqueous solution involves 82 solute species, including 26 species of ore-forming elements (Cu^+, $CuOH^0$, $Cu(HS)_2^-$, $Cu(HS)_2H_2S^-$, $CuOHCl^-$, $CuCl^0$, $CuCl_2^-$, $CuCl_3^{2-}$, Cu^{2+}, Zn^{2+}, $ZnOH^+$, $Zn(OH)_2^0$, $ZnHCO_3^+$, $Zn(HS)_2^0$, $ZnCl^+$, $ZnCl_2^0$, $ZnCl_3^-$, $ZnCl_4^{2-}$, $ZnSO_4^0$, Pb^{2+}, $PbOH^+$, $Pb(HS)_2^0$, $PbCl^+$, $PbCl_2^0$, $PbCl_3^-$, and $PbCl_4^{2-}$). The list of possible solid phases contains 54 minerals (Table 1, main rock-forming, metasomatic, and ore minerals).

The calculations were carried out for a temperature of 370°C and a pressure of 1 kbar. The country granite was chosen to be equivalent to the granite of the Kholst Massif (SiO_2 = 71.75, Al_2O_3 = 13.98, Fe_2O_3 = 0.105, FeO = 2.333, FeS = 0.0525, TiO_2 = 0.37, P_2O_5 = 0.19, MgO = 0.66, MnO = 0.06, CaO = 0.96, Na_2O = 3.00, K_2O = 4.965, S = 0.06, LOI = 1.612 wt %). According to our analyses, the background concentrations of ore elements in the granites were as follows (wt %): Zn = 0.004, Pb = 0.003, and Cu = 0.002. The primary hydrothermal solution was assumed to contain 0.5 *m* H_2CO_3, 1.0 *m* NaCl, and 0.1 *m* HCl.

The results of the simulations (two series of calculations) of the composition of the initial mineralizing solution are shown in Figs. 8 and 9. Series 1 (Fig. 8) included the calculations of a single act of interaction in the system granite–primary solution at different rock masses in the reactor (0.01–10 kg) and a constant mass of the solution (1 kg of H_2O). This methodological

approach is most often employed in thermodynamic simulations, but, as will be demonstrated below, it can constrain only the lower boundary of the possible concentrations of ore components. Series 2 of our calculations (Fig. 9) simulated multiple interactions between a number of portions (waves) of the primary solution and a rock that was modified as a result of these interactions.

It was established that an increase in the rock mass in the reactor (an increase in the rock/water ratio, R/W in Fig. 8) brings about an increase in the concentrations of metals in the equilibrium solution (dissolution without crystallization of ore minerals in the altered rock) and their subsequent drastic decrease to a level corresponding to equilibrium with galena, sphalerite, chalcopyrite, or bornite and the minerals of altered granites. With an increase in the reacting rock mass, the concentration of sulfide sulfur in the solution also increases.

These processes are coupled with changes in the equilibrium mineral assemblage: the contents of quartz, muscovite, and albite decrease, that of microcline gradually increases, and sulfides appear (first, galena and, then, bornite, which gives way first to chalcopyrite, then to sphalerite, and, at higher rock/water ratios, to pyrrhotite).

As can be seen from Fig. 8, the system granite–solution at 370°C, 1 kbar can serve as a source of ore-forming components and sulfide sulfur for the initial fluid. However, the highest concentrations attained in these calculations are equal to 5.4×10^{-4} *m* for Zn, 4.5×10^{-5} *m* for Pb, and 8.5×10^{-5} *m* for Cu. The dependence of the concentrations of ore elements on the rock and solution mass ratio can characterize the evolution of the composition of the initial mineralizing solution. The involvement of progressively greater rock masses in the leaching reactions with time (an increase in the R/W ratio) should cause the concentrations of ore-forming components to pass through a maximum (the typical R/W ratios of such systems range from 0.2–0.5 to 10).

Series 2 of our calculations (Fig. 9) amplifies and complements series 1. Thirty portions of the primary solution successively "pass" through the reactor containing 10 kg of granite (this corresponds to R/W = 10 in Fig. 8). The changes in the system involve a dramatic increase in the concentrations of metals: by a factor of 12 for Zn, from 1.9×10^{-4} to 2.3×10^{-3} *m*; by a factor of 17 for Pb, from 1.7×10^{-5} to 2.9×10^{-4} *m*; and by a factor of 27 for Cu, from 1.3×10^{-5} to 3.5×10^{-4} *m*. The pH of the solution (5.3), its ionic strength, and major-element composition remain practically unchanged. The increase in the concentrations is caused by a decrease in the overall amount of sulfide sulfur in the system (because of its extraction) and a decrease in its concentration in the equilibrium solution.

The trajectories of increasing concentrations of metals terminate as soon as the dissolving minerals are fully leached from the reservoir (which depends on the clarkes of ore elements in granites). For example sphalerite, whose solubility is the highest, completely disappears from the equilibrium assemblage with the passage of ten solution portions, while galena and Cu minerals disappear only after 20 portions. Pyrrhotite is the first sulfide to disappear during leaching. The occurrence of this mineral in the equilibrium assemblage during stages 1–6 constrains the increase in the solubility of ore sulfides. This is expressed in the form of plateaus in the concentration trajectories for Zn, Pb, and Cu (analogously, see Fig. 8 at R/W of approximately 10). An increase or decrease in the starting rock mass in the reactor results, respectively, in the lengthening or shortening of the plateau at the preservation of the tendency toward an increase in the concentrations. The minimum in the Pb leaching curve is accounted for by a switch from hydrosulfide to chloride complexes. The drastic decrease in the Cu concentration (waves 1 and 2) is brought about by a change in the equilibrium phase assemblage (the appearance of Fe-poorer epidote). The phase composition of granite after its reaction with 15 portions of the primary solution does not change as drastically: the content of quartz increases by 2.5 wt %, muscovite increases by 3%, albite by 5%, and the microcline content decreases by 9%. The calculation results demonstrate that (1) the concentrations of metals in the leaching solutions can attain values more than one order of magnitude higher than the respective concentrations after a single interaction act (up to $n \times 10^{-3}$ *m* for Zn and $n \times 10^{-4}$ *m* for Pb and Cu); (2) the concentrations of metals in the solutions significantly vary in the course of the leaching processes (Zn predominates early in this process, subsequently the Pb and Cu concentrations become higher, and eventually the solution becomes barren during the final stages); (3) the concentration of sulfide sulfur in the solutions ranges from $n \times 10^{-2}$ to $n \times 10^{-3}$ *m* and is high enough for sulfides to start crystallizing if conditions change.

These results demonstrate that ore-bearing solutions can evolve in the root portions of ore deposits even without changes in the external parameters (*T*, *P*, and the primary solution composition). The mineralizing solution composition depends on the duration (number of solution waves in our models) of reactions in the junction zone between solution conduits and ore-controlling tectonic structures (for example, large regional faults and their auxiliary shear and extension faults hosting mineralized veins). Of course, every act of tectonic reactivation brings about changes in the junction zone, such as rejuvenation (reopening) of filtration pathways for the primary solution. Obviously, the leaching of metals can take place within solution-conducting structures (the main pathways of the primary solutions), but the degree of interaction between the solutions and country rocks is low (low R/W ratios, Fig. 8), and, correspondingly, the concentrations of metals and sulfur are not high either. At best, solutions of this type can produce mineralized zones but not economic ore concentrations, a feature commonly attributed to the main ore conduit structures of ore fields.

Additional materials and comparison of the leaching intensities of metals (U and Pb) from a variety of rocks are reported in Chapters 3–5 within the framework of certain models for ore genesis. In this section, we emphasize the fairly complicated but also quite efficient character of the mobilization of ore-forming components from rocks.

2.5. Conclusions

(1) Comparison of the results of our physicochemical simulations of interactions in the rock–water system demonstrates that the study of even simple models makes it possible to identify and predict geochemical phenomena that take place in natural systems of rocks and thermal groundwaters.

(2) High hydrogen partial pressures can result from high-temperature interactions between water and basic rocks and do not necessarily require any additional endogenic hydrogen source.

(3) The closeness of the concentrations of elements occurring in nature and obtained in the simulations depends on the temperature, geochemical properties of the elements, and the rock/water ratio. The higher the temperature, the closer the actual concentrations to their calculated values. The same effect can be achieved by increasing the rock/water ratio; i.e., the effects of temperature and the rock/water ratio are similar.

(4) It is demonstrated that interaction between the primary barren solutions and granites may give rise to mineralized solutions that can produce ore-forming hydrothermal systems.

(5) The interaction of barren hydrothermal fluids of constant composition with granites brings about a significant increase in the concentrations of ore-forming elements (as high as $n \times 10^{-3}$ to $n \times 10^{-4}$ *m* for Zn, Pb, and Cu) in the leaching solutions without any changes in the external conditions. The metalliferous potential of these solutions significantly varies in the course of the mobilization process.

(6) The concentration of sulfide sulfur in the leaching solutions ranges from $n \times 10^{-2}$ to $n \times 10^{-3}$ *m*, i.e., values sufficiently high for sulfides of ore elements to form if the conditions change. These data indicate that there is no need for any other sources of sulfide sulfur for the origin of the bulk of sulfides at vein base-metal deposits.

PART 2: GENESIS OF ORE MINERALIZATION UNDER NEARLY ISOTHERMAL CONDITIONS

Models of ore genesis are discussed in this section in the order of a systematic complication of the physicochemical conditions in the ore-forming systems:

* a model for U mineralization in a chemically homogeneous medium with heterogeneous filtration properties at constant *T* and *P* (as exemplified by the Chauli deposit);

* a model for U mineralization in areas composed of rocks of contrasting chemical composition at constant *T* and *P* (deposits of unconformity type).

CHAPTER 3 ORIGIN OF ORE MINERALIZATION IN A MEDIUM WITH UNEQUAL FILTRATION PROPERTIES AND A HOMOGENEOUS CHEMICAL COMPOSITION

The analysis of the paleohydrodynamic conditions under which the hydrothermal ore mineralization was produced indicates that these conditions pervasively affected the development of zoning at these deposits, which comprise cutting bodies of disseminated and stringer mineralization localized in compositionally relatively homogeneous country rocks with contrasting filtration properties [Barsukov *et al.*, 1977]. This type includes large hydrothermal deposits that developed under nearly isothermal conditions in continental volcanotectonic depressions, as exemplified by the Chauli deposit of U–Mo ore association. The deposit was exhaustively examined and described in much detail by Barsukov *et al.* [1972] and is used in this publication as a representative object for thermodynamic modeling. The paleohydrodynamic reconstructions of the solution pathways at the deposit during the mineral stage yielded schemes similar to those for other deposits of this type and can be further employed for constructing an equilibrium–dynamic model for this deposit.

3.1. Brief Characterization of the Chauli Deposit

The Chauli deposit consists of a series of ore zones, which are closely spaced arrays of mineralized fractures above an area of the local sagging basement blocks of the depression. The U–Mo mineralization is constrained exclusively to the middle volcanotectonic liparite unit (P_2), whose stratigraphy comprises three members. Each of the members is made up of intercalating lava and pyroclastic material of different permeability. During the mineral stage, the mineralized zones were a single steeply dipping ore chimney cutting across all members of the middle liparite unit from its bottom to top (Fig. 10.I). The mineralized veins in the fractures and related disseminated ores are dominated by pitchblende, calcite, and sulfides (pyrite, galena, sphalerite, molybdenite, and others) and contain subordinate amounts of coffinite, chlorite, sericite, and iron oxides (goethite and hematite). The mineralized veins are surrounded by aureoles of hydrothermally altered host rocks, whose main, most clearly pronounced zone is that of argillization (with the development of montmorillonite and kaolinite).

The following variations in characteristics of the deposit were identified in its vertical cross section: